Ore Geology Reviews 72 (2016) 149–164

Contents lists available at ScienceDirect

Ore Geology Reviews

journal homepage: www.elsevier.com/locate/oregeorev

The origin of the gold and uranium ores of the Black Reef Formation, Transvaal Supergroup, South Africa

S. Fuchs [a,*], A.E. Williams-Jones [a], W.J. Przybylowicz [b,c]

[a] Department of Earth and Planetary Science, McGill University, 3450 University Street, Montreal, QC H3A 0E8, Canada
[b] Materials Research Department, iThemba LABS, National Research Foundation, P.O. Box 722, Somerset West 7129, South Africa
[c] AGH University of Science and Technology, Faculty of Physics & Applied Computer Science, Al. A. Mickiewicza 30, 30-059 Krakow, Poland

ARTICLE INFO

Article history:
Received 9 April 2015
Received in revised form 14 July 2015
Accepted 16 July 2015
Available online 17 July 2015

Keywords:
Black Reef
Gold
Uranium
Hydrothermal reworking
Witwatersrand

ABSTRACT

The Black Reef Formation is a laterally extensive sedimentary succession at the base of the Transvaal Supergroup. The quartz-pebble conglomerates host erratic concentrations of gold and uranium; however, in areas that are located spatially above the gold and uranium-bearing reefs of the Witwatersrand Supergroup, the concentrations can reach ore-grade. Although the depositional environment was similar to that of the Witwatersrand Supergroup, the processes that lead to the high gold and uranium concentrations in the Black Reef were quite different. The Black Reef experienced intense, post-depositional hydrothermal alteration by circulating aqueous and hydrocarbon fluids (oils) that deposited large volumes of native gold, uranium minerals and pyrobitumen. The gold, which is filamentous, is concentrated along As–Ni-rich surfaces of pyrite, and with uraninite in pyrobitumen. In both environments, the gold is interpreted to be the product of chemically-triggered precipitation from hydrothermal fluid(s). The uraninite occurs either as precipitates in pyrobitumen or is "invisible" in the pyrite, occurring as nanoparticles in this mineral. This indicates that conditions were sufficiently oxidizing for the hydrothermal transport of uranium, and contrasts with the case for the Witwatersrand reefs where much of the uranium is detrital. Luminescent radiation damage associated with vein quartz and pyrobitumen, as well as the diffuse distribution pattern of uranium in the pyrobitumen may indicate that some uranium was transported by liquid hydrocarbons. Pyrite in the Black Reef (sedimentary, detrital and hydrothermal pyrite) is highly enriched in gold, uranium and other redox-sensitive trace elements. Provenance analyses using the trace element compositions of the pyrite show that it was not the result of erosional reworking of the underlying Witwatersrand Reefs. However, the close spatial association of high gold and uranium concentrations in the Black Reef with ore-bearing Witwatersrand reefs suggests strongly that gold and uranium, whether in pyrite or occurring as native gold and uraninite, were hydrothermally recycled (uranium may have been recycled by hydrocarbon fluids) from the Witwatersrand Reefs.

1. Introduction

The Black Reef Formation is a thin, but laterally extensive succession of siliciclastic rocks at the base of the Neoarchaen to Paleoproterozoic Transvaal Supergroup. The quartz-pebble conglomerates of the Black Reef Formation host erratic gold and uranium concentrations associated with a variety of ore minerals including pyrite, pyrrhotite, sphalerite, galena and chromite (Frey, 1988). Locally, the gold and uranium concentrations are of ore grade, and have been mined on a small-scale since the late 1950s (Henry and Master, 2008). Although, in many respects, the Black Reef is indistinguishable from the gold–uranium-bearing Witwatersrand reefs, and its depositional environment is similar (Barton and Hallbauer, 1996), the genetic relationship of the gold and uranium mineralization of the Black Reef to that of the Witwatersrand Supergroup, if any, is still unclear.

The two widely discussed genetic models for the gold–uranium ores of the Witwatersrand Supergroup are: 1) that they are paleo-placers modified by hydrothermal processes (Frimmel, 1997; Frimmel et al., 2005; Kirk et al., 2002; Minter, 2006; Minter et al., 1993; Pretorius, 1991); and 2) they are of entirely hydrothermal origin (Barnicoat et al., 1997; Law and Phillips, 2005; Phillips and Law, 1994; Phillips et al., 1997; Phillips and Myers, 1989). According to the latter model, uranium and organic matter infiltrated the basin synchronously (Law and Phillips, 2005) or in separate events (Barnicoat et al., 1997). Recently, it also has been proposed that the gold is entirely syngenetic, having been precipitated by algal mats from surface waters and shallow seas (Frimmel and Hennigh, 2015; Heinrich, 2015). Whether any of these models apply to the Black Reef Formation is unknown.

The Black Reef gold mineralisation was first described by Graton (1930) and Swiegers (1939) who, based on the observation of auriferous

* Corresponding author.
E-mail address: sebastian.fuchs@mail.mcgill.ca (S. Fuchs).

http://dx.doi.org/10.1016/j.oregeorev.2015.07.010
0169-1368/

quartz veins, interpreted it to be of hydrothermal origin. Subsequent sedimentological studies, however, led to the conclusion that the Black Reef, including much of its gold mineralization, was derived by erosion from the underlying Witwatersrand Reefs (Frankel, 1940; Papenfus, 1964; Spellman, 1986). Germs (1982), for example noted that gold concentrations are high proximal to the underlying reefs of the Central Rand Group of the Witwatersrand Supergroup, and that the gold occurs preferentially with minerals of detrital origin on sedimentary surfaces (e.g., bedding planes and cross beds). According to the sedimentary reworking hypothesis, parts of the Black Reef with high gold grades therefore correspond to parts of the underlying reefs endowed with gold, and those with uneconomic concentrations to parts that were barren of gold.

A later mineralogical study, however, cast doubt on the sedimentary reworking interpretation (Frey, 1988). Noting the high variability in the nature and proportion of the pebbles relative to that of the heavy minerals, and an absence of corresponding changes in the sorting and grain sizes of the detrital components, Frey (1988) concluded that the sediments of the Black Reef had multiple sources, i.e., they were not the products of simple reworking of the underlying Witwatersrand reefs. He also noted an intimate association of gold of low fineness ($Au_f = (Au + 1000)/(Au + Ag)$), in the range of 500 to 800, to clearly epigenetic and hydrothermally formed minerals, such as sphalerite, galena and Fe–Ni–Co-sulphides, which suggested that some of the gold, at least, was of hydrothermal origin. Further evidence against the sedimentary reworking hypothesis was provided by a study comparing the morphology and composition of detrital pyrite in the Black Reef to that of detrital and recrystallized (epigenetic) pyrite in the underlying Kimberley Reef of the Central Rand Group (Barton and Hallbauer, 1996). The detrital pyrite grains in the Black Reef are much larger than either the detrital or later recrystallized pyrite grains of the Kimberly Reef. Moreover, they have lower proportions of radiogenic lead (low $^{207}Pb/^{204}Pb$, $^{206}Pb/^{204}Pb$ ratios) and lower proportions of ^{238}U than the Kimberly Reef pyrites, as well as higher total Pb and lower total U concentrations.

Although the more recent studies have rejected the sedimentary reworking hypothesis for the Black Reef, and there is some evidence that hydrothermal processes may have played a role in metal concentration, no consensus has emerged on the genesis of the gold and uranium mineralization in the Black Reef Formation. In this paper, we use a variety of analytical methods to determine the distribution of gold and uranium and associated minerals in the Black Reef, the mineralization style and history, and the relationship between the Black Reef and the underlying Kimberly Reef. Based on these data, we propose a model in which both the gold and the uranium of the Black Reef were recycled hydrothermally (and perhaps by hydrocarbon liquids in the case of uranium) from the underlying reefs of the Witwatersrand Supergroup.

2. Geological setting

The Transvaal Supergroup is located in the Transvaal Basin in South Africa, and rests on the northern and western parts of the Kaapvaal Craton (Fig. 1). The Black Reef Formation is the basal lithostratigraphic unit of the late Archean to early Proterozoic Transvaal Supergroup (Els et al., 1995). It lies unconformably on the volcano-sedimentary rocks of the Ventersdorp Supergroup and the sedimentary succession of the Witwatersrand Supergroup, and is the youngest Formation within the basin that contains economic concentrations of gold. The sedimentary rocks of the Black Reef Formation were deposited under mainly fluviatile conditions and in a later shallow epicratonic marine environment (Button, 1973; Els et al., 1995; Obbes, 2000). Onset of a marine transgression led to the deposition of the basal black shale of the overlying Chunispoort Group, which grades conformably into a sequence of dolomites, cherts and limestones (Clendenin et al., 1991; Eriksson and Reczko, 1995; Henry et al., 1990). As was the case for the Witwatersrand reefs, potential provenance areas for Black Reef sediment were located in the north, northeast and west of the basin, and the paleo-current flow was strongly controlled by existing paleo-channels and valleys (Barton and Hallbauer, 1996; Button, 1973; Germs, 1982). Henry and Master (2008) estimated the age of Black Reef Formation to be 2.59 Ga in the Johannesburg area on the basis of an ion microprobe (SHRIMP) zircon age of 2.709 Ga ± 4 Ma for felsic rocks of the underlying Venterdorp Supergroup (Armstrong et al., 1991) and a zircon age of 2.588 Ga ± 7 Ma for the basal unit of the overlying Chunispoort group (Martin et al., 1998).

The Black Reef Formation generally consists of massive to cross-bedded, weakly metamorphosed quartz arenites, clay and siltstones, carbon-rich shales and minor conglomerates that form an upward-fining sequence with a quartzite-rich lower unit containing variably developed auriferous conglomerates, grits or scattered pebbles grading into the overlying, commonly carbonaceous shale-rich unit (Frey et al., 1991). The East and West Rand sub-basins, which locally are characterized by economic gold concentrations, were the result of deep erosion of the topographic surface, with paleo-channels incising the underlying Witwatersrand and poorly developed Ventersdorp rocks (Barton and Hallbauer, 1996). In the East Rand, three different Black Reef facies types can be distinguished within these channels: i) the Channel Facies, ii) the Blanket Facies — Basal Unit and iii) the Blanket Facies — Pyrite Leader Unit (Fig. 2). Regional metamorphism subsequently affected the Black Reef, and was accompanied by widespread alteration due to fluid migration induced by the emplacement of the Bushveld Igneous Complex (c. 2.06 Ga) or the Vredefort impact (c. 2.02 Ga) (Coward et al., 1995; Robb and Meyer, 1995). Studies of the Witwatersrand Supergroup indicate greenschist facies conditions with peak temperatures between 300° and 400 °C (Frimmel, 1994; Phillips, 1988; Phillips and Law, 1994).

3. Sample sites and descriptions

The basal quartz–pebble conglomerates of the Black Reef Formation were identified and sampled from pre-existing drill-core collections as well as current mining operations. For this study, specimens were selected from the northern and north-western Transvaal, the eastern Transvaal (near Kaapsehoop), the northeast part of Johannesburg, in the Klerksdorp and Carletonville goldfields (southwest of Potchefstroom and east of Orkney), the northern parts of the Welkom gold fields, the West Rand and East Rand, and the eastern extension of the East Rand sub-basin (Fig. 1). The thickness of the conglomerates (if developed) varies from a few centimetres in the northern and eastern parts of the basin to several metres in the East and West Rand sub-basins. The size, proportion and distribution of quartz pebbles in the conglomerates vary considerably at the different locations together with the grade of the Au–U mineralization. In the East Rand sub-basin, the Black Reef occurs in N–S trending channels that incised the strata of the Witwatersrand Supergroup. The lowermost, Channel Facies, consists of large quartz boulders in a medium-grained dark quartzite matrix, and is overlain by the Basal unit of the Blanket Facies, a massive upwards-fining sequence of medium-grained quartzites with cross-bedded alternating bands of pyrite (Fig. 2). The uppermost facies, the Pyrite Leader, is characterized by a high content of pyrite, commonly in excess of 80 vol.%.

The stratigraphically lower Au–U-pyrite-bearing Kimberley Reef (Witwatersrand Supergroup) and B-Reef (Witwatersrand Supergroup) were sampled for provenance studies. The Kimberley Reef consists of alternating quartzites, conglomerates and intercalated shales, and is mined together with the Black Reef in the East Rand. The B-Reef is a quartz-pebble conglomerate with intercalated chert, jasper pebbles and minor shales, bound by siliceous to slightly argillaceous rocks, and was sampled from mining operations in the Welkom gold field.

4. Methodology

Whole-rock concentrations of gold and uranium were analysed by fire assay and acid-digestion ICP–OES/MS at ACME Labs Canada, with detection limits of 0.5 ppb for gold and 0.5 ppm for uranium. For the

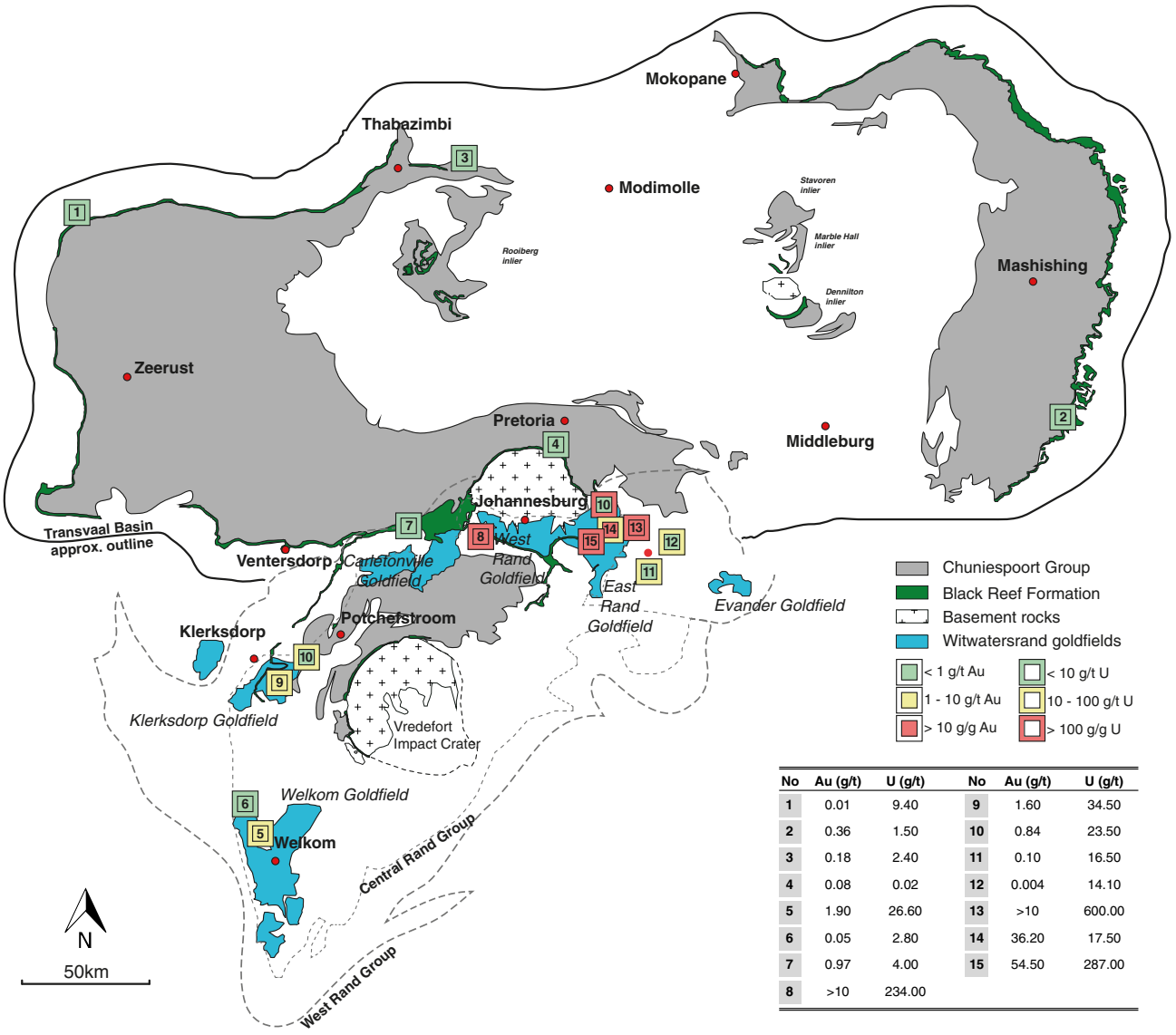

No	Au (g/t)	U (g/t)	No	Au (g/t)	U (g/t)
1	0.01	9.40	9	1.60	34.50
2	0.36	1.50	10	0.84	23.50
3	0.18	2.40	11	0.10	16.50
4	0.08	0.02	12	0.004	14.10
5	1.90	26.60	13	>10	600.00
6	0.05	2.80	14	36.20	17.50
7	0.97	4.00	15	54.50	287.00
8	>10	234.00			

Fig. 1. A simplified geological map of the Transvaal Supergroup, including the Witwatersrand goldfields, showing gold and uranium concentrations of the Black Reef conglomerates (modified after Eriksson et al., 2006). The numbered boxes are colour-coded to reflect metal grade (green = low, yellow = moderate, high = high grade) with the numbers corresponding to the numbers in the inset table of gold and uranium concentrations. (For interpretation of the references to colour in this figure legend, the reader is referred to the web version of this article.).

mineralogical and mineral chemical study, selected rock samples were embedded in epoxy resin and glued on glass slides, and prepared as uncovered, polished thick / thin sections. The samples were studied with a standard petrographic light microscope and optical cathodoluminescence microscope. Back-scattered electron images and the major element chemistry of the pyrite were obtained using a JOEL 890 electron microprobe (EPMA) equipped with one EDS and five WDS detectors at McGill University. Appropriate mineral standards were used for instrument calibration and operated with a 20 kV acceleration voltage, 20 nA current and <1 μm spot size.

An Agilent 7700x quadrupole ICP–MS at the Geological Survey of Canada equipped with a Photon-Machines Analyte 193 excimer laser ablation system and a Helex ablation cell was used for trace element analysis. Spot analyses were performed at 10 Hz, an energy of ~4 J/cm^{-2} and a beam size of 43 μm on suitable grains. Line scans were conducted with a 5 μm/s scanning speed and a 25 μm beam size and a pre-ablation step. The sulphide standards, PO689, PO726 (both produced at Memorial University, St. Johns, Canada), MASS1 (Wilson et al., 2002) and the basalt glass standard, GSD-1G (Jochum et al., 2011), were used for calibration and a multi-standard approach (bracketing analyses) with Fe as an internal standard evaluated by previous electron microprobe analyses. The GLITTER™ software package was used for selective signal integration and the calculation of element concentration and detection limits.

Micro-PIXE analyses were performed using the nuclear microprobe at the Materials Research Department of iThemba LABS, Somerset West, South Africa. The facility uses a 6 MV single-ended Van de Graaff accelerator and Oxford magnetic quadrupole triplet for beam focusing (Prozesky et al., 1995). A proton beam of 3.0 MeV energy and ~2 nA current was focused to a 5 × 5 μm^2 spot and raster-scanned over selected areas of samples, using square or rectangular scan patterns of variable sizes (up to 2.5 mm × 2.5 mm) and a variable number of pixels (up to 128 × 128). PIXE spectra were registered with a Si(Li) detector (30 mm^2 active area, working distance 24 mm), positioned at a take-off angle of 135°. The effective energy resolution of the PIXE system (for the Mn Kα line) was 155–160 eV, measured for individual spectra. The X-ray energy range was set between 1 and 42 keV. The data acquisition system uses CAMAC and VME bus modules and XSYS software running on a VAX-4000 computer, linked with a PC running program written in LabVIEW for the control of specimen stage stepper motors, magnetic scanning coils and the beam-on-demand deflection coils

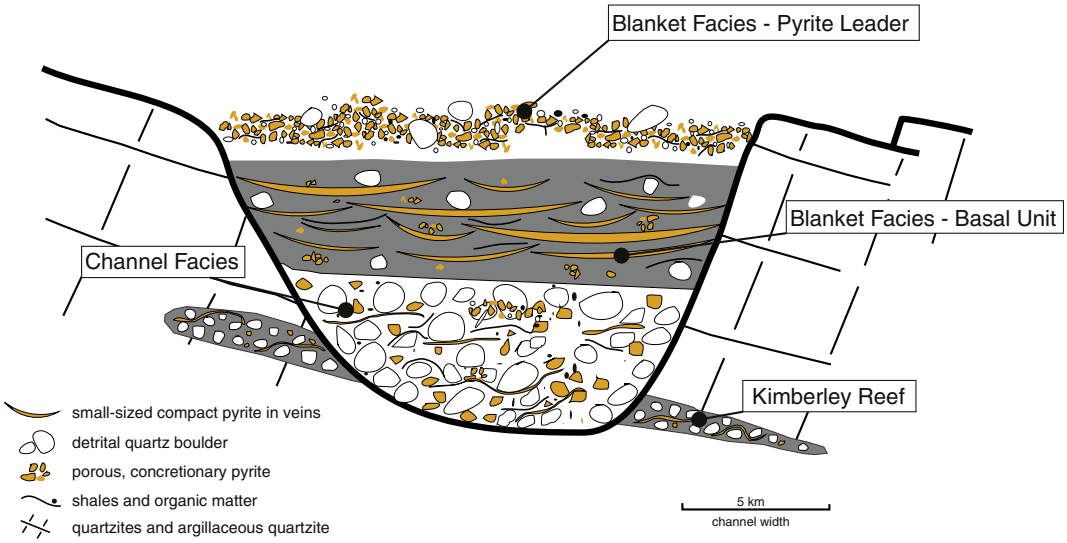

Fig. 2. A cross-section of the Black Reef facies types that incise the underlying Kimberley Reef of the Witwatersrand Supergroup in the East Rand basin (modified from Barton and Hallbauer, 1996).

(Churms et al., 1993, 1999). The normalization of results was done using the integrated beam charge collected from the insulated specimen holder.

Each selected area was measured twice using two different X-ray absorbers interposed between the sample and PIXE detector. Application of the thicker absorber (150 μm Al) restricted the practical X-ray energy range to above 4 keV. Additional measurements of low-energy X-rays (between 1–4 keV) were made using a 125 μm thick Be absorber. The proton current in this case was ~500 pA in order to reduce the number of pile-ups in the PIXE spectra.

Quantitative results were obtained using a standardless method employing GeoPIXE II software (Ryan, 2000; Ryan et al., 1990). The calibration of the analytical system was tested by measurements of reference materials; pure elements, pure minerals and USGS (United States Geological Survey) standards BIR-1 and BCR-2. Element mapping was performed using the Dynamic Analysis method (Ryan, 2000; Ryan and Jamieson, 1993; Ryan et al., 1995), which generates element images using a series of X-ray lines (in this case K, L or M lines). The maps are (i) overlap-resolved, (ii) with subtracted background and (iii) quantitative, i.e., reported in ppm or wt. % units. Maps were constructed from five analysed areas in the selected Black Reef samples using individual average matrix compositions from scanned areas obtained from EPMA analyses. Line traverses across interesting areas were also made. In addition, PIXE spectra were extracted from smaller regions of arbitrarily selected shapes within maps. PIXE spectra from these regions were fitted using a full nonlinear deconvolution procedure (Ryan et al., 1990), employing matrix compositions corresponding to regions.

5. Results

5.1. Basin-wide gold and uranium distribution

Black Reef conglomerates were analysed throughout the Transvaal basin for their gold and uranium contents. Fig. 1 shows the distribution of gold and uranium in the Black Reef at different locations as colour-coded boxes plotted on the map and the corresponding mean concentrations (table inset). All samples contain detectable amounts of gold and uranium. The highest gold and uranium concentrations, up to 54.5 g/t gold and 600 g/t uranium, were found in samples from the West and East Rand basins/goldfields. Low concentrations were measured in samples that originated from the northern, north-western and eastern parts of the basin. Low to moderate concentrations were detected in the conglomerates that originated from the Klerksdorp and Carletonville goldfield (1.6 g/t Au, 34.5 g/t U max.), Welkom goldfield (1.9 g/t Au, 6.4 g/t U max.) and the eastern extension of the East Rand goldfield (0.1 g/t Au, 16.5 g/t U max.). Gold and uranium concentrations are both highest where the Black Reef is located proximal to the underlying Witwatersrand Reefs (e.g., in the East and West Rand), whereas concentrations are lowest distal to Witwatersrand Reefs.

5.2. Mineralogy

5.2.1. Ore mineralogy

The quartz–pebble conglomerates of the Black Reef Formation contain a wide variety of ore minerals, namely pyrite, chromite, zircon, rutile, chalcopyrite, arsenopyrite, gersdorffite, colbaltite, pyrrhotite, galena, sphalerite, uraninite, brannerite, monazite, xenotime-(Y) and native gold. As in the conglomerates of the Witwatersrand reefs, pyrite is the most abundant ore mineral in the Black Reef and can be classified into different types based on its morphology. A detrital compact, rounded pyrite (often referred as “detrital, compact or massive pyrite”) is the dominant type, and occurs as spherical, sub-rounded to rounded grains with abraded edges and a massive internal texture (Fig. 3A, C, D, F, G, H, I). This pyrite-type is non-porous, mainly inclusion-free, but rarely contains chalcopyrite and pyrrhotite inclusions. A detrital, rounded, concretionary, porous pyrite-type, often referred to as “(syn)sedimentary, reworked pyrite” or “buckshot pyrite” (Barton and Hallbauer, 1996; Ramdohr, 1958; Saager, 1970; Utter, 1978) is abundant in the Black Reef conglomerates of the East and West Rand basin (especially in the Blanket Facies). This pyrite-type has the largest grain-size of any pyrite-type in the Black Reef (up to 7 mm in diameter) and its morphology is highly variable, with grains ranging from relatively compact, slightly porous, and rounded with clear boundaries to highly porous with irregular boundaries (Fig. 3A, B, F, H). The pores commonly contain sericite (muscovite) and quartz; larger pores and healed fractures commonly host sphalerite, chalcopyrite and gold inclusions (Fig. 3C, D). Some of the grains of this pyrite-type have obvious internal lamellar structures and rarely, concentric porous and compact zones (i.e., a porous core, a compact inner rim, and a porous outer rim). Dark varieties of the concretionary pyrite, referred to as sooty and mudball pyrite, that can be distinguished by their highly porous, fractured morphology and/or desiccation cracks are observed locally (Fig. 3G, H). The dark appearance is due to numerous hydrocarbon and sericite inclusions. A third pyrite-type, epigenetic pyrite (often referred to as “recrystallized” or “hydrothermal” pyrite), is less abundant than the other two pyrite-types, and occurs mainly as overgrowths on pre-existing pyrite grains

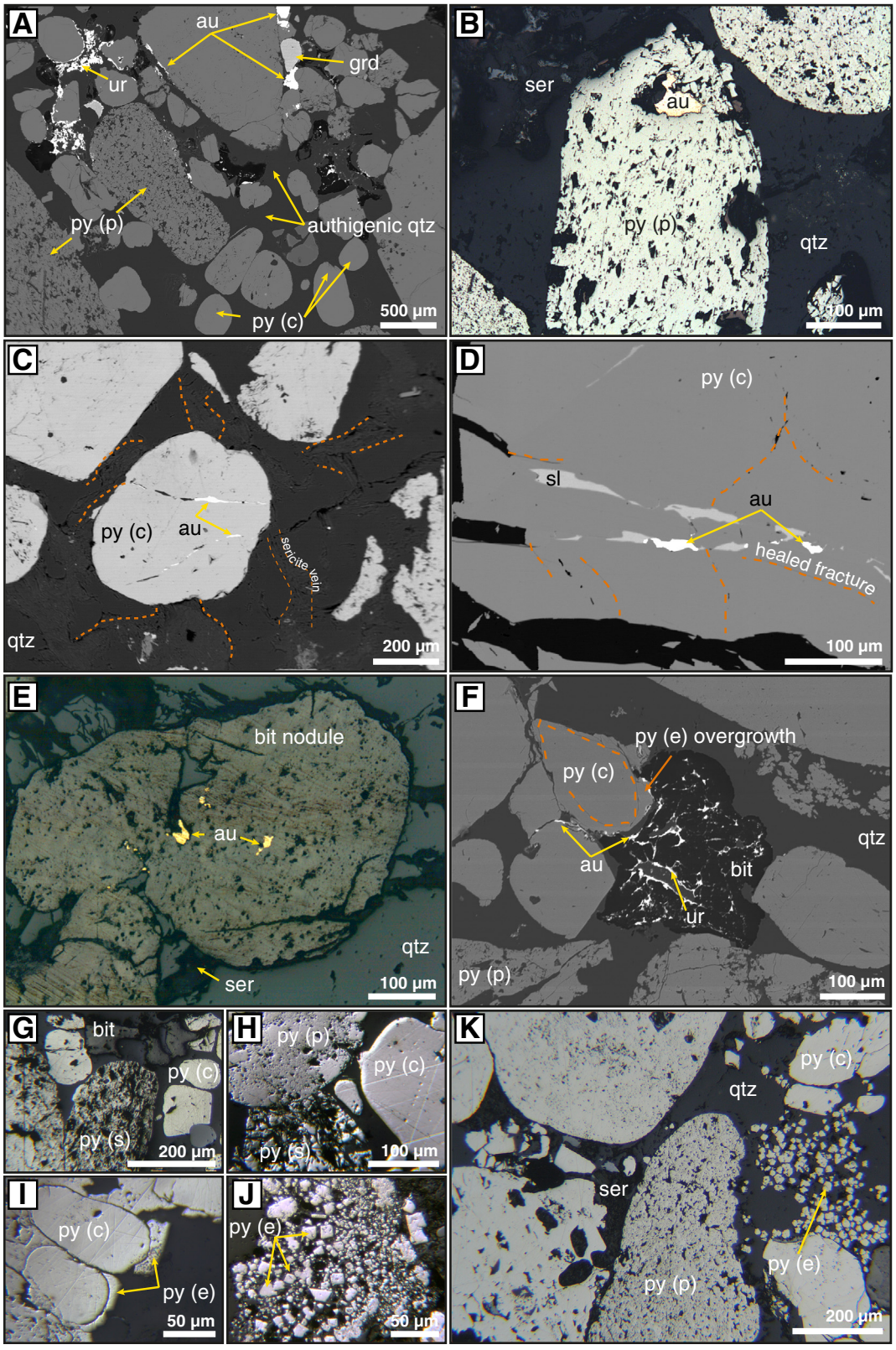

Fig. 3. Back-scattered electron (A, D, F) and reflected light microscopy (B, C, E, G–K) images of samples of the Black and Kimberley Reef conglomerates in the East Rand sub-basin. A) Rounded compact and concretionary pyrite in authigenic quartz cement from the Pyrite Leader Facies. B) Native gold inclusion in a pore of a concretionary pyrite grain. C) Compact pyrite containing native gold in fractures. The pyrite grains are cemented by authigenic quartz cut by veins filled with sericite (mainly muscovite, dashed orange lines). D) Healed fractures in compact pyrite containing sphalerite and native gold. E) Pyrobitumen nodules with inclusions of native gold. The nodules are surrounded by a mantle of sericite and sericite-bearing veins in authigenic quartz. F) Pyrobitumen nodule containing uraninite in veins and as inclusions accompanied by native gold at the rim. Native gold is also present in overgrowths of pyrite on compact pyrite. G, H) Sooty pyrite in association with compact and concretionary pyrite; the dark colour is due to hydrocarbon and sericite inclusions. I) Epigenetic pyrite overgrowths on cores of compact pyrite. J) Euhedral, epigenetic pyrite grains in the Blanket Facies of the Black Reef. K) Kimberley Reef containing compact, concretionary and epigenetic varieties of pyrite. Abbreviations: au = native gold; bit = pyrobitumen; grd = gersdorffite; qtz = quartz; py (c) = compact pyrite; py (e) = epigenetic pyrite; py (p) = concretionary pyrite; py (s) = sooty pyrite; ser = sericite; sl = sphalerite; ur = uraninite. (For interpretation of the references to colour in this figure legend, the reader is referred to the web version of this article.).

(Fig. 3I), but also as individual, euhedral crystals (Fig. 3J), that rarely exceed 15 μm in diameter.

The rounded compact, as well as the rounded concretionary pyrite-types are also observed in the Kimberly Reef (Fig. 3K), although not the sooty variety of the concretionary pyrite-type. Epigenetic pyrite is ubiquitous and occurs in groups of small euhedral crystals (Fig. 3K). Henceforth, the pyrite-types described above will be referred to as: i) compact pyrite, ii) concretionary pyrite, iii) sooty pyrite (including mudball pyrite) and iv) epigenetic pyrite.

The samples of the Black Reef from the East Rand have been studied in greatest detail as they contain the highest concentrations of gold and uranium (Fig. 1). The gold grains in the Black Reef are irregular to dendritic rather than being rounded micro-nuggets, suggesting that they are of hydrothermal origin. A significant proportion of the gold is present as rims on pyrite and Ni–Co–Fe–sulpharsenide crystals or fills interstices between them (Fig. 3A, F). Some gold fills larger pores in the concretionary pyrite (Fig. 3B). Much of the gold, however, occurs in fractures in the compact and concretionary pyrite (Fig. 3C, D). Where this is the case, the pyrite is associated with sericite-filled veins in the quartz matrix. Most of the gold-bearing fractures are healed and filled with recrystallized pyrite and sphalerite (Fig. 3D). Solitary pyrobitumen nodules, often referred to as "fly-speck carbons" (Drennan and Robb, 2006) occur along fractures in the conglomerates in association with quartz and phyllosilicates, and are 200–700 μm in diameter. The nodules frequently contain native gold and uranium minerals (mainly uraninite and brannerite). Significantly, the latter are limited to pyrobitumen nodules (Fig. 3F). Moreover, in contrast to the underlying Witwatersrand reefs, where much of the uraninite is rounded and detrital, in the Black Reef, the uraninite is irregularly shaped and usually does not exceed 10 μm in diameter.

An optical microscope was used to record the frequency of gold occurrences in relation to the textural environment of samples from the East Rand sub-basin (Fig. A.1). Approximately 76.1% of the gold is associated with pyrite and 21.4% with pyrobitumen, 2.2% is within the authigenic quartz matrix, and only 0.4% within the quartz pebble framework.

5.2.2. Rock-forming minerals

Cathodoluminescence microscopy (CL) was used to investigate the nature of the quartz in relation to gold and uranium in the Black Reef, and to distinguish detrital from authigenic quartz. The majority of the rounded, detrital grains in the Black Reef conglomerates display intense, homogenous blue colours. Individual grains vary from dark to lighter blue and are characterized by sutured boundaries (Fig. 4A). Some grains are purple to dark purplish brown, and show an internal zonation of luminescence colours (Fig. 4B). In conglomerates with a mainly quartz-pebble framework (e.g., Channel or Blanket Facies), brown and weakly luminescent authigenic quartz can be clearly distinguished from detrital quartz. It forms overgrowths on detrital quartz cores or fill voids in fractured grains (Fig. 4B). The contacts between the detrital cores and overgrowths are commonly sutured. In conglomerates with a framework of pyrite grains and less abundant detrital quartz, authigenic quartz occurs as a homogeneous matrix with purplish to reddish brown luminescence colours, and commonly encloses detrital grains of quartz, pyrite, chromite or zircon (Fig. 4C, D). The purplish brown luminescence colours of the authigenic quartz change to bright orange in zones close to open or healed fractures (Fig. 4D, E, G). These fractures intersect authigenic quartz and locally detrital ore minerals (e.g., pyrite, Fig. 4G). They are filled with syntaxial muscovite (Fig. 4J, K) that replaced detrital quartz, and very fine-grained quartz (chert or opal). Thin veinlets of pyrobitumen, which line the fractures (Fig. 4J), provide evidence that liquid hydrocarbons migrated with hydrothermal solutions. Fibrous quartz has been observed in larger fractures (Fig. 4K) with sericite and pyrobitumen as well as in pressure shadows of rigid pyrite grains. The intense orange-brown luminescence colours (Fig. 4E, G) along these alteration zones can be attributed to radiation damage, showing that the migrating fluids carried radioactive elements. Bright orange halos around uraniferous pyrobitumen nodules and to a lesser extent pyrite display the greatest evidence of radiation damage (Fig. 4G).

5.3. Pyrite chemistry

5.3.1. Trace element concentrations

Recent studies of the B-Reef, Carbon Leader Reef, Elsburg Reef, Vaal Reef and Ventersdorp Contact Reef (Agangi et al., 2013; Koglin et al., 2010; Large et al., 2013) have shown that LA–ICP–MS trace element analysis is an effective tool with which to characterise the Witwatersrand pyrite. The following suite of trace elements, Al, Si, Ti, V, Cr, Mn, Co, Ni, Cu, Zn, As, Se, Y, Zr, Mo, Sn, Sb, Te, Ba, Hf, Ta, W, Au, Tl, Pb, Bi and U, was analysed by LA–ICP–MS and used to characterise the compact, concretionary and sooty varieties of pyrite in the Black Reef. Owing to their small grain-size, it was not possible to analyse the epigenetic pyrite. The same analyses were carried out on the different pyrite-types of the underlying Kimberley Reef and the B-Reef of the Witwatersrand Supergroup for comparison (Section 5.3.2).

Spot LA–ICP–MS analyses revealed that the compact pyrite in the Black Reef has a very low gold concentration (max. 0.62 ppm; mean 0.14 ppm Au; Fig. 5) and the lowest trace element concentration of all pyrite analysed in this reef. Only Co, Ni, Cu and As have concentrations exceeding 100 ppm (133 ppm Co, 212 ppm Ni, 137 ppm Cu and 364 ppm As; mean values, Table 1). Gold concentrations in the concretionary pyrite are significantly higher, in the range of 0.11 ppm to 1.95 ppm (mean 0.71 ppm Au, Fig. 5). The other trace metals also have higher concentrations than in the compact pyrite. The following trace elements in the concretionary pyrite have concentrations in excess of 100 ppm: As (1199 ppm), Ni (984 ppm), Pb (478 ppm), U (402 ppm), Co (359 ppm) and Sb (128 ppm); mean values, (Table 1). The sooty pyrite has slightly higher gold concentrations, in the range of 0.74 ppm to 2.01 ppm (mean 1.16 ppm Au, Fig. 5). The trace metal concentrations are similar to those of the concretionary pyrite grains, but are higher for As (1763 ppm), Ni (1211 ppm), Zn (230 ppm), Cr (175 ppm), Sb (175 ppm) and U (169 ppm; mean values, Table 1).

The element pairs As–Au, Sb–Au, As–Ni, Cr–Mn and Pb–Bi in all types of Black Reef pyrite all display positive correlations on binary plots (Fig. 6A, B, D, E F). Gold shows a weak positive correlation with U in compact pyrite, whereas the Au content of concretionary and sooty pyrite is independent of uranium content (Fig. 6C). These diagrams facilitate the visualisation of the trace element signatures of the three types of pyrite. On all diagrams, the compact detrital pyrite is distinguished by its low concentration of gold and other trace metals relative to the other pyrite-types. It is noteworthy, that the Au–As concentrations of all three pyrite-types plot below the gold saturation line of Reich et al. (2005), indicating that the gold occurs as a solid solution in the pyrite rather than as nanoparticles. The absence

Fig. 4. Cathodoluminescence (A to E, G), reflected-light (F, H) and transmitted-light (J, K) microscope images of samples of the Black Reef. A) Detrital quartz grains in homogenous blue and dark blue luminescence colours. B) Dark blue to purple detrital quartz grains overgrown by mauve authigenic quartz. C) Blue detrital quartz grains in a fine-grained quartz matrix (purplish brown colours). D) High-grade gold and uranium sample of the Pyrite Leader Facies containing orange-brown authigenic quartz and detrital quartz grains (blue-coloured grains). (E, F) Detrital quartz (dark blue) cemented by an authigenic quartz matrix (orange to brown luminescence colours) in a high-grade sample hosting pyrite, pyrobitumen (nodules), gold and uranium. The anomalous luminescence colours surrounding the pyrobitumen nodules (and also weakly around pyrite) indicate radiation damages. Fractures are highlighted by white dashed lines. (G, H) A high-grade sample containing pyrobitumen. Intense radiation damage is evident by orange luminescence adjacent to fractures (white dashed lines) passing close to pyrobitumen nodules. (J) A vein containing fined-grained, sericite, quartz and pyrobitumen. (K) Fibrous quartz in a vein with sericite at its margins. Abbreviations: bit = pyrobitumen; py (c) = compact pyrite; qtz = quartz; py (p) = concretionary pyrite; ser = sericite. (For interpretation of the references to colour in this figure legend, the reader is referred to the web version of this article.).

of sub-microscopic inclusions is also indicated by the presence of broad flat rather than spikey Au-peaks in the profiles of LA–ICP–MS spot analyses.

5.3.2. Trace element distributions

LA–ICP–MS line scan analyses were performed to determine the distribution of invisible gold and associated trace metals within individual

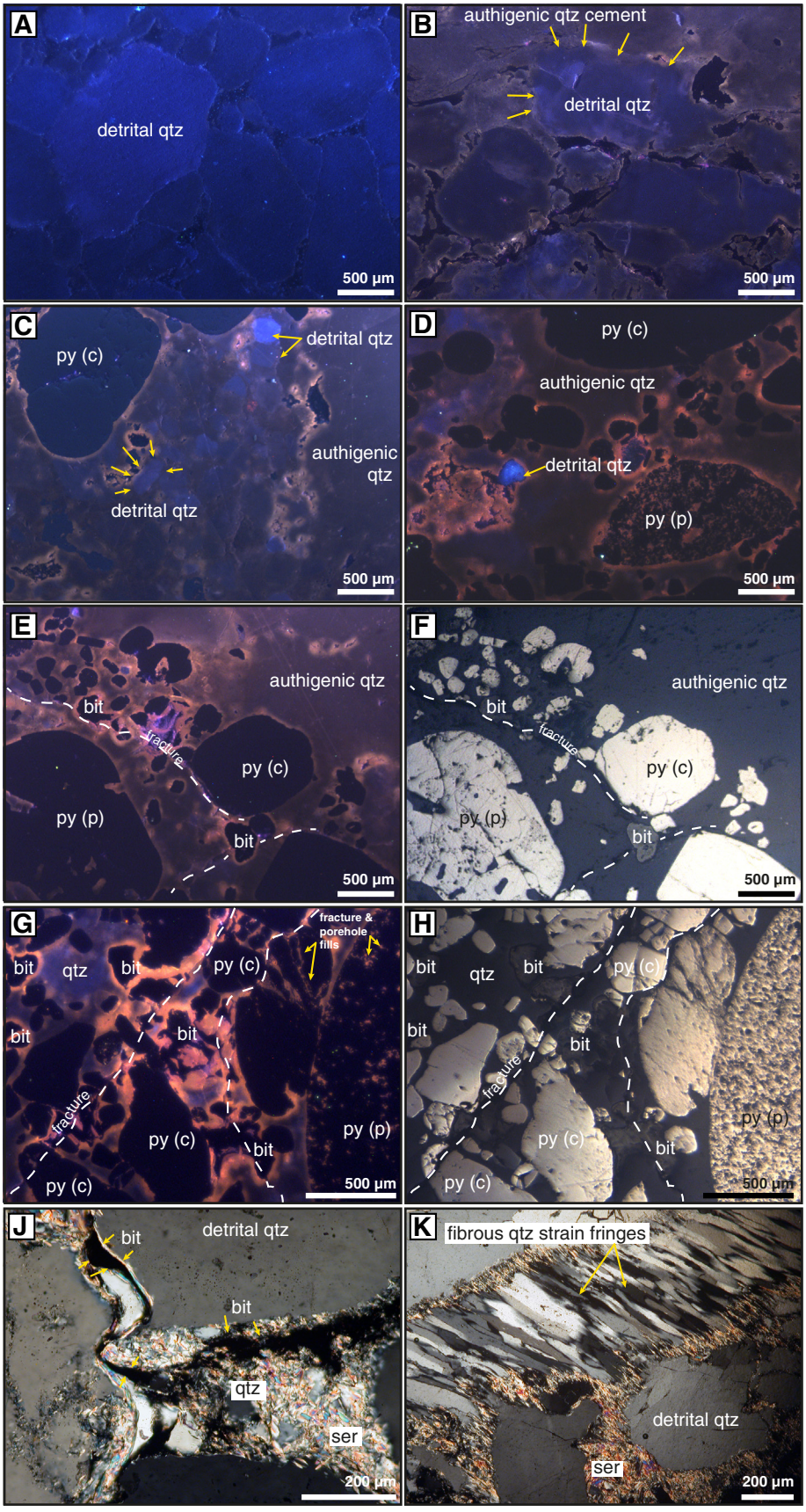

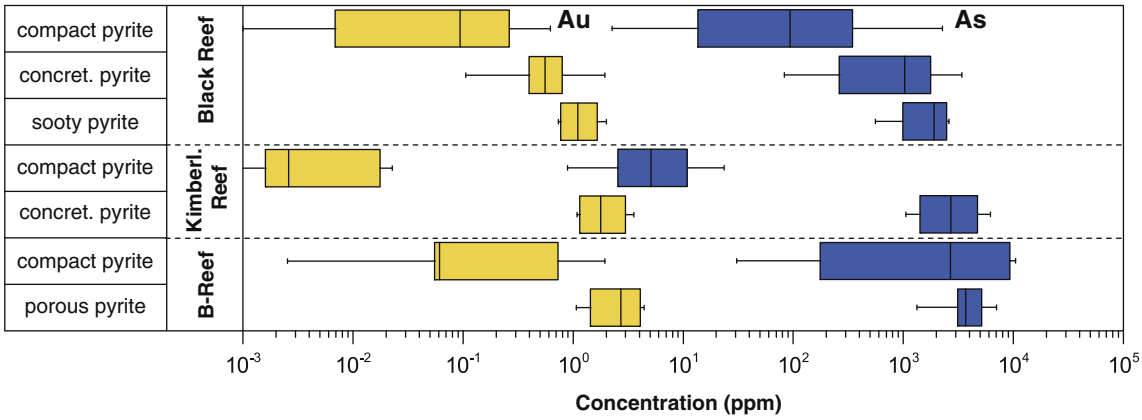

Fig. 5. Box-whisker plot showing the distribution of gold and arsenic in compact, concretionary and sooty types of pyrite in the Black Reef, Kimberley Reef and B-Reef. The boxes show the second and third quartiles (25–75%) and the median, and the whiskers the minimum and maximum values of the dataset.

pyrite grains. Fig. 7A and B provide examples of continuous traverse lines ablated through a concretionary pyrite and a compact pyrite with an epigenetic overgrowth, respectively. The line scan across the concretionary pyrite (Fig. 7A) exhibits an inhomogeneous gold distribution with concentrations varying by two orders of magnitude. Concentrations are highest in the core and at the rim, and low between these zones. The same distribution is observed for cobalt, nickel, arsenic, antimony, tellurium, lead and bismuth, explaining the positive correlations between gold and the trace metals illustrated in Fig. 6. In contrast to gold, uranium concentration climbs from the core to the rim. Moreover, between the core and rim zones, where the gold concentration dips and peaks, the uranium concentration is anomalously high and low, respectively. This indicates that uranium was incorporated in the pyrite differently from gold (the possibility that the peaks in uranium concentration reflect larger inclusions can be ruled out by the uniformly high Fe concentration). Surprisingly, the lead distribution does not parallel that of uranium (radiogenic) and instead mimics the profile for gold. This suggests that radiogenic lead derived from pre-existing uraninite was incorporated into the pyrite structure together with gold (and the other trace metals) and was not coupled with uranium. The cyclic variation and broad peaks (rather than spikes) without a pronounced core-rim zoning for gold and the other trace metals, except uranium, have been observed in all analysed concretionary pyrite. This indicates an episodic uptake of these metals during pyrite growth.

The distribution of gold and other trace elements in the compact pyrite (core) and the epigenetic overgrowth (rim) is quite different from that in the concretionary pyrite (Fig. 7B). Gold concentration is low in the core of the compact pyrite, increases outwards, then decreases to its initial level as the core-rim boundary is approached (the maximum counts were an order of magnitude lower than in the concretionary pyrite). The other trace elements, except Ni and Co have similar distributions. Cobalt and nickel are high in the core of the compact pyrite and decrease steadily to its rim. The epigenetic rim is highly enriched in gold (the counts are four orders of magnitude higher than for gold in the concretionary pyrite) as well as uranium and other trace elements. Tellurium and bismuth decrease sharply from their

Table 1
Mean, median, minimum and maximum contents of trace elements in the different pyrite types of the Black Reef. Values corrected for single outliers are marked with an asterisk.

Concentration	Black Reef: compact pyrite				Black Reef: concretionary pyrite				Black Reef: sooty pyrite			
(ppm)	Mean	Median	Min	Max	Mean	Median	Min	Max	Mean	Median	Min	Max
Ti47	41.32	4.29	0.62	371.46	*850.92	946.54	2.82	2472.29	863.15	253.61	66.60	1969.36
V51	1.21	0.44	0.02	6.76	12.57	6.24	1.08	66.99	26.25	16.12	6.73	66.73
Cr53	15.75	1.69	0.38	147.56	94.16	38.63	3.67	385.91	174.84	176.12	24.74	361.96
Mn55	6.82	1.44	0.22	41.94	85.72	36.09	1.17	926.82	48.87	31.43	9.91	90.87
Co59	*132.85	52.53	0.08	879.93	358.84	246.09	16.46	1238.94	328.37	220.59	97.17	1439.45
Ni60	211.57	117.02	3.02	742.71	984.05	694.31	54.35	4390.45	1211.25	1003.14	648.89	2143.33
Cu65	137.41	19.81	0.18	924.17	97.74	67.45	16.16	491.92	68.05	73.03	24.96	110.87
Zn66	52.84	2.40	0.63	491.33	*81.98	14.63	1.69	862.28	229.60	56.95	5.89	1247.34
As75	363.56	93.18	2.26	2264.64	1198.84	1029.49	83.00	3396.61	1763.03	1907.08	559.58	2600.28
Se77	23.42	17.91	0.71	97.76	36.57	23.68	4.41	108.69	20.23	11.70	3.37	72.93
Y89	0.58	0.05	0.00	2.47	7.53	4.41	0.05	28.53	6.34	7.49	0.66	15.66
Zr90	17.85	0.15	0.00	162.07	62.67	39.74	0.41	236.42	40.14	11.49	2.40	101.03
Mo95	4.12	0.02	0.02	12.32	2.33	0.14	0.02	28.72	6.44	6.32	0.12	13.76
Sn118	0.13	0.08	0.02	0.35	0.88	0.92	0.06	2.27	0.83	0.51	0.27	1.84
Sb121	14.71	1.27	0.01	93.73	128.30	59.05	2.58	377.53	175.22	116.63	40.82	368.90
Te125	5.56	0.39	0.03	50.33	3.76	0.66	0.09	23.08	3.59	1.26	0.77	14.08
Ba137	2.45	0.29	0.01	10.64	20.18	9.82	0.22	135.83	49.76	42.31	4.67	107.65
Hf177	0.45	0.01	0.00	3.30	1.34	0.89	0.01	4.69	0.97	0.30	0.08	2.58
Ta181	0.03	0.00	0.00	0.21	2.76	0.22	0.00	38.76	0.36	0.05	0.01	0.90
W182	0.12	0.01	0.00	1.41	0.97	0.73	0.02	5.91	0.83	0.38	0.06	2.03
Au197	0.14	0.09	0.00	0.62	0.71	0.56	0.11	1.95	1.16	0.87	0.74	2.01
Tl205	0.11	0.05	0.00	0.72	2.00	0.25	0.04	12.33	4.17	2.17	0.29	11.68
Pb208	*83.62	14.44	0.01	584.76	478.45	435.42	65.95	1475.04	472.83	487.34	149.96	713.85
Bi209	3.74	0.46	0.02	36.50	28.52	5.31	0.06	215.47	25.69	18.57	8.94	51.22
U238	6.32	1.01	0.00	74.61	402.21	36.84	0.05	3752.06	168.71	46.68	0.06	651.18

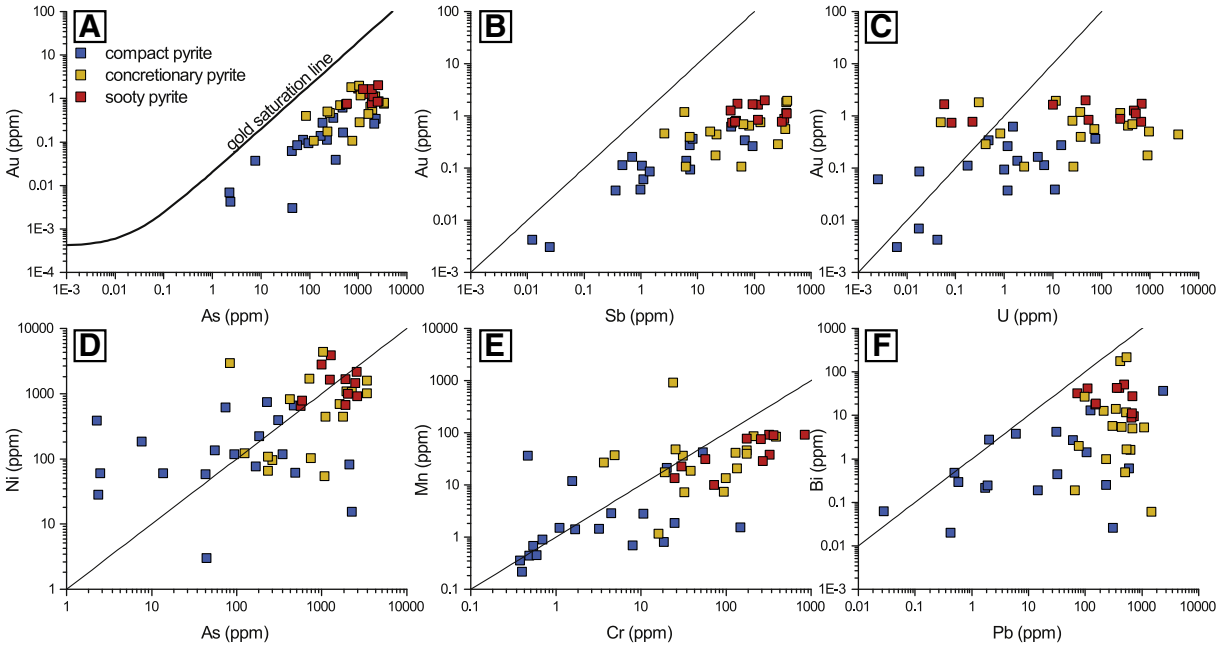

Fig. 6. Binary plots of the element pairs As–Au (A), Sb–Au (B), U–Au (C), As–Ni (D), Cr–Mn (E) and Pb–Bi (F) for compact, concretionary and sooty pyrite types in the Black Reef. The gold saturation line in A was taken from Reich et al. (2005).

concentrations in the adjacent compact pyrite rim. These data confirm that the epigenetic overgrowth formed in a very different environment from that of the compact and concretionary pyrite types.

5.4. Comparisons to Kimberly and B Reef pyrites

The trace element chemistry of the compact and concretionary pyrite in the Kimberley Reef was analysed by LA–ICP–MS for purposes of comparison to the Witwatersrand. A smaller set of pyrite samples from the B-Reef of the Witwatersrand Supergroup (in the Welkom goldfield) was also analysed to further represent Witwatersrand pyrite. Discriminant analyses were performed on the trace element data (Cr, Mn, Co, Ni, Cu, Zn, As, Se, Sb, Te, Au, Pb, Bi and U) for the two pyrite types from these reefs and the Black Reef using the statistical software package SAS JMP® 11. These analyses make use of multivariate statistics to predict differences among groups of samples (e.g., minerals from different localities) based on characteristic common variables (e.g., chemical composition), and involve determination of the minimum number of dimensions needed to describe these differences. For the purposes of visualization, the multivariate means and individual sample points are plotted in the two dimensions (2-axis canonical plot) which best separate the groups.

The results of the discriminant analyses for both the compact pyrite (Fig. 8A) and concretionary pyrite (incl. sooty pyrite, Fig. 8B) show that pyrite from the Black Reef, Kimberly Reef and B-Reef form separate clusters, indicating that they represent geochemically distinct populations. Most data points plot within the confidence contours of the mean of the canonical scores at the 95% confidence level and the contours of the 50% normal distribution. However, there are a few outliers because of the high chemical variability of each population. The compact and concretionary pyrites of the B-Reef are loaded on the first discriminant axis with values greater than 14 and 4, respectively, and are distinct from the corresponding Black Reef and Kimberley Reef pyrites that have low scores on the first discriminant axis. The compact pyrite of the Black Reef and Kimberley Reef have scores loaded on the second discriminant axis, that range from 1.8 to 5.2 in the Black Reef, and from −2.2 to 1.5 in the Kimberley Reef. The concretionary pyrite has second discriminant axis values from −1.7 to 1.8 in the Black Reef and from 2.8 to 5.2 in the Kimberley Reef (Fig. 8A, B). The data points for concretionary and sooty pyrite in the Black Reef overlap, indicating that the sooty pyrite very likely is a subtype of concretionary pyrite.

5.5. Native gold and pyrite

Quantitative compositional micro-PIXE maps and back scattered electron (BSE) images were prepared to investigate the textural and compositional characteristics of native gold that occurs in association with pyrite and pyrobitumen. The BSE images of gold occupying fractures in pyrite (Fig. 9A, E), on pyrite (Fig. 9E) and in pyrite pores (Fig. 9I) indicate that the gold is texturally younger than the host pyrite.

The micro-PIXE element maps show that there is a direct spatial association between high As and Ni concentrations and the location of the native gold (compare Fig. 9C with Fig. 9D, F with Fig. 9G and H, and Fig. 9J with Fig. 9K and L). This is also illustrated by comparing the BSE image in Fig. 9A with the depth-penetrating micro-PIXE line scan in Fig. 9B. In all cases, the gold is located adjacent to peaks of As and Ni in the pyrite. In these areas, the concentrations of As (up to 5920 ppm) and Ni (up to 3760 ppm) significantly exceed the amounts of As and Ni, that are associated with the invisible gold in pyrite (Fig. 9A). The As and Ni-rich zones form rims in the pyrite around pores containing gold (Fig. 9K) or line gold-bearing fractures (Fig. 9G, H).

5.6. Native gold/uraninite and pyrobitumen

In addition to its association with pyrite, native gold is intimately associated with pyrobitumen and uranium minerals. This is illustrated in two micro-PIXE elemental map sets (Fig. 10A –F, G –O). The gold may be enclosed in the pyrobitumen (Fig. 10E), but also commonly occurs on the margins of pyrobitumen nodules (Fig. 10L). By contrast, the uranium minerals are almost invariably within the pyrobitumen (Fig. 10F, M). Small amounts of other metals, such as Fe, Ni and Cu may also be present in the pyrobitumen nodules (Fig. 10H, J, K), suggesting mobilisation and (re-) precipitation of phases containing these metals. The major U-mineral in the Black Reef is irregularly shaped uraninite that in many cases is indistinguishable from its finely dispersed and intergrown alteration minerals (i.e., brannerite, coffinite and xenotime). The micro-PIXE maps show that U, Pb and Y are homogeneously distributed within the pyrobitumen (Fig. 10 M, N, O),

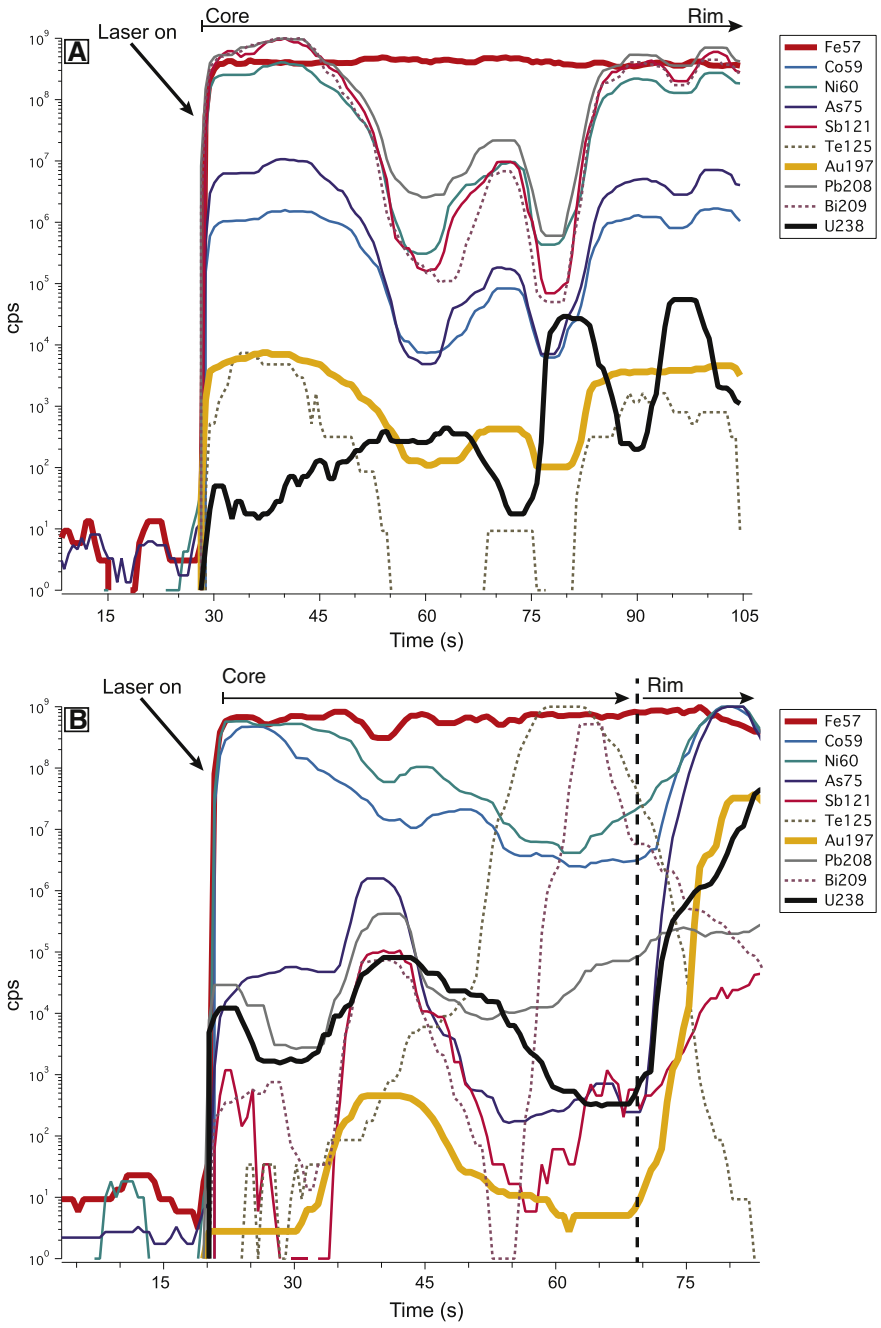

Fig. 7. Time-resolved LA–ICP–MS line scan across: A) Concretionary pyrite and B) a compact pyrite core with an epigenetic pyrite overgrowth. The concretionary pyrite shows a cyclic variation of Au counts that correlates with those of other elements, except that of U, which vary antithetically. (B) Counts for gold and uranium also vary cyclically in the compact pyrite core but, in contrast to the concretionary pyrite, uranium counts vary sympathetically with those of gold. Counts for both metals increase sharply in the overgrowth.

indicating the presence of uraninite and xenotime-(Y). Some of the U, Pb and Y may be hosted by nanoparticles within the pyrobitumen nodules, as the distribution of these elements in the pyrobitumen nodules cannot be fully explained by the minerals displayed in the back-scattered image (Fig. 10G).

6. Discussion

6.1. Introduction

The gold and uranium grades of the conglomerates of the Black Reef vary as a function of location in the Transvaal basin (Fig. 1). The highest concentrations are in the Witwatersrand goldfields, reaching 54.5 g/t gold and 600 g/t uranium, whereas they are low outside the goldfields, usually <1 g/t and 10 g/t, respectively. This relationship has been long recognised and led to the hypothesis that the Black Reef formed by sedimentary-erosional reworking of the underlying Witwatersrand reefs (Frankel, 1940; Germs, 1982; Papenfus, 1964; Spellman, 1986). The latter was supported by the observation that deeply incised paleo-channels (e.g., in the East Rand sub-basin), which eroded the Witwatersrand strata, contain high concentrations of gold and uranium. However, as has already been noted, this hypothesis is not supported by the sedimentology or the grain-size and isotopic composition of the pyrite (Barton and Hallbauer, 1996; Frey, 1988). By contrast, the relationships mentioned above are consistent with the hypothesis that the gold and uranium were hydrothermally recycled from the underlying Witwatersrand reefs. Below, we will make the case that hydrothermal (and hydrocarbon) fluids associated with metamorphic

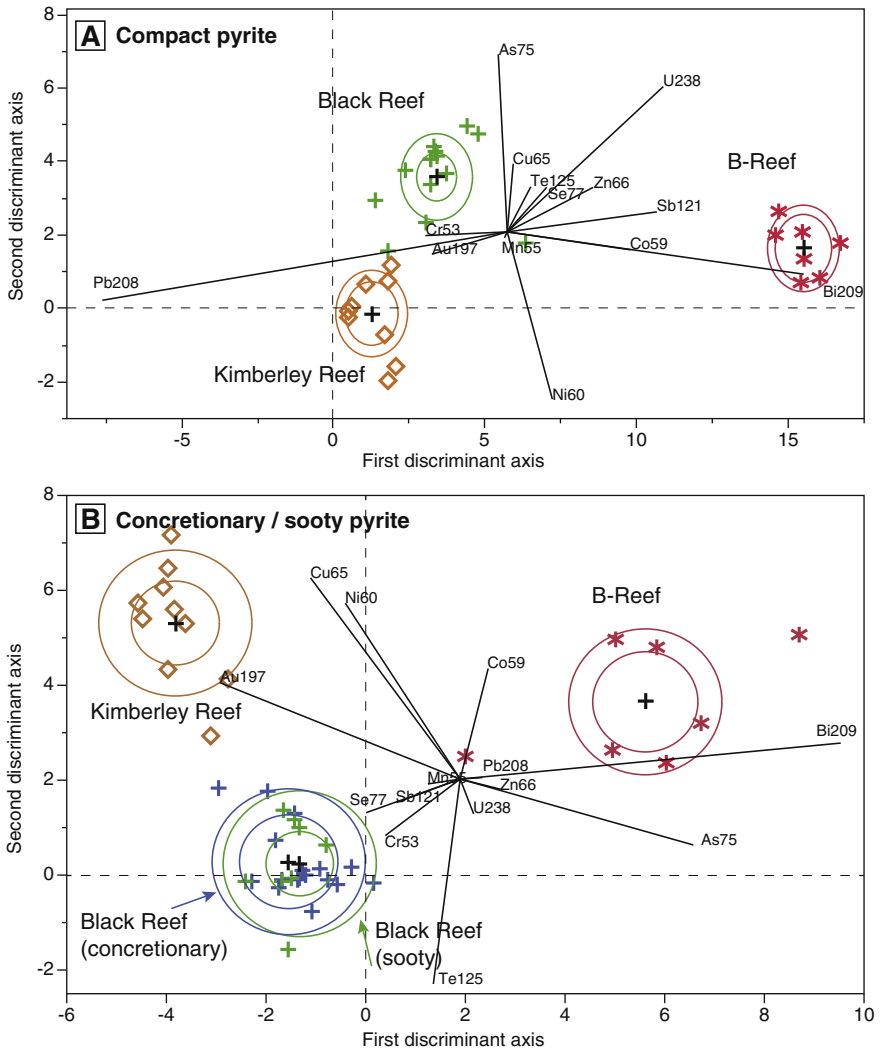

Fig. 8. Multivariate discriminant diagrams for A) compact pyrite and B) concretionary (incl. sooty) pyrite from the Black (green/blue), Kimberley (orange) and B Reefs (red). All compact and concretionary groups of pyrite represent geochemically distinct populations. Smaller ellipsoids indicate the confidence contours of the mean of canonical scores at the 95% confidence level, the larger ellipsoids the contours of the 50% normal distribution and the black crosses the canonical mean values of each population.

and thermal events (e.g., emplacement of the Bushveld Complex and the Vredeford impact event) that affected the Witwatersrand Supergroup ascended along structural pathways, and transported gold and uranium into the Black Reef Formation.

6.2. The origin of the detrital pyrite

The multivariate discriminant analyses of the most abundant trace elements in compact pyrite (Fig. 8A) and concretionary/sooty pyrite (Fig. 8B) from the Black Reef, Kimberley Reef and B-Reef provide convincing evidence that both detrital pyrite-types of the Black Reef are different from the detrital pyrite of the Kimberley Reef and other Witwatersrand Reefs. With the exception of a few isolated outliers, the detrital pyrites from the three reefs have separate fields of provenance and are thus each set is geochemically distinct. It therefore follows that the detrital pyrites of the Black Reef could not have been derived from the underlying Witwatersrand reefs by erosion, although they likely formed by a similar process.

Although, the distribution of the trace elements in pyrite of the Black Reef is different from those of pyrite in the underlying Kimberley and B Reefs of the Witwatersrand Supergroup, all carry the same complement of trace elements (for reefs other than those referred to in this study, see Agangi et al., 2013; Koglin et al., 2010; Large et al., 2013). In all of these reefs, the compact pyrite is characterized by very low concentrations of Au and trace elements that commonly substitute into the pyrite lattice. This is an indication that the compact pyrite of the Black Reef formed under conditions and/or in environments similar to compact pyrite in the Witwatersrand Supergroup, however, the ultimate source of this pyrite is still unclear. Previous studies have interpreted the compact pyrite to have been derived from felsic and/or mafic rocks in greenstone belts of the Archean hinterland that may have hosted orogenic gold deposits (Barton and Hallbauer, 1996; Frimmel et al., 2009; Koglin et al., 2010).

In contrast to the compact pyrite, the concretionary and sooty pyrites of the Black Reef and underlying Witwatersrand reefs are all characterized by high concentrations of Au, U, Co, Ni, As, Sb, Cr, Te, Pb and Bi (Figs. 5 and 6, Table 1). Moreover, the Au is zonally distributed and Co, Ni, As, Sb, Te, Pb and Bi have similar distributions to Au (Fig. 7A). This indicates that these elements were incorporated during the growth of the pyrite and that their incorporation was episodic. Such trace element incorporation is typical of pyrite forming in carbonaceous shales and mudstones (Coveney, 2000; Large et al., 2007, 2011; Meyer and Robb, 1996; Piper and Calvert, 2009; Wood, 1996; Wronkiewicz and Condie, 1987), and suggests that the concretionary and sooty pyrite may be of sedimentary/diagenetic origin. During sedimentation, the metals would have been adsorbed from seawater onto organic matter/microorganisms and subsequently incorporated into the pyrite structure during diagenesis (Large et al., 2007). As the Au

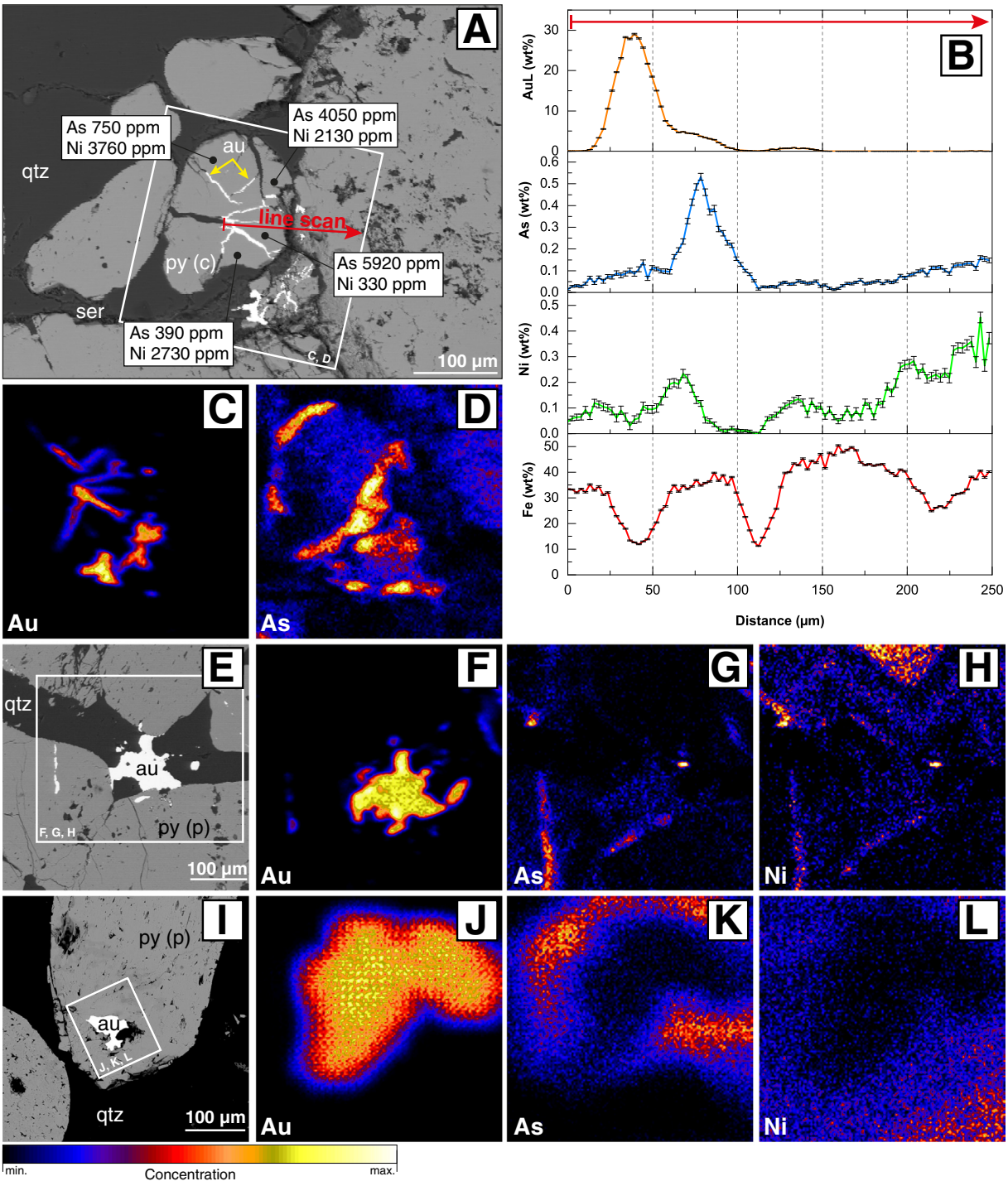

Fig. 9. (A) A Back-scattered electron image showing a compact pyrite grain containing fractures filled by native gold. Also shown are the As and Ni contents of selected points in the grain. (B) A scan showing the distribution of selected elements along a line indicated by the red arrow shown in A; bars on the scan show the 2σ error in the element concentrations. (C and D) Micro-PIXE maps for Au and As of the area shown by the square in A. (E) Back-scattered electron image of native gold in authigenic quartz cementing two concentric pyrite grains. (F–H) Micro-PIXE maps for Au, As and Ni of the area shown by the square in E. (I) Back-scattered electron image of native gold in a concentric pyrite grain. (J–L) Micro-PIXE maps for Au, As and Ni of the area shown by a square in I. Abbreviations: au = native gold; py (c) = compact pyrite; py (p) = concretionary pyrite; ser = sericite; qtz = quartz. (For interpretation of the references to colour in this figure legend, the reader is referred to the web version of this article.).

concentrations are below the gold saturation line of Reich et al. (2005) (Fig. 6A), the gold is most likely held in solid solution in the pyrite ("invisible gold"). This is also probably true of the other trace elements referred to above, given their very similar distributions relative to gold. The very different distribution of uranium from that of gold and the other trace elements (Fig. 7A) implies a different mechanism of uranium incorporation. As uranium ions are much larger and have much higher charge than those of gold and the other trace elements they probably did not fit easily in the pyrite structure and, instead, uranium may have been incorporated in the concretionary pyrite as uraninite nanoparticles. Such nanoparticles have been observed in pyrobitumen in the Carbon Leader of the Witwatersrand Supergroup (Fuchs et al., 2015) and could have been transferred to the pyrite from organic matter in the mudstone/shale during diagenesis. A nanoparticle source for the

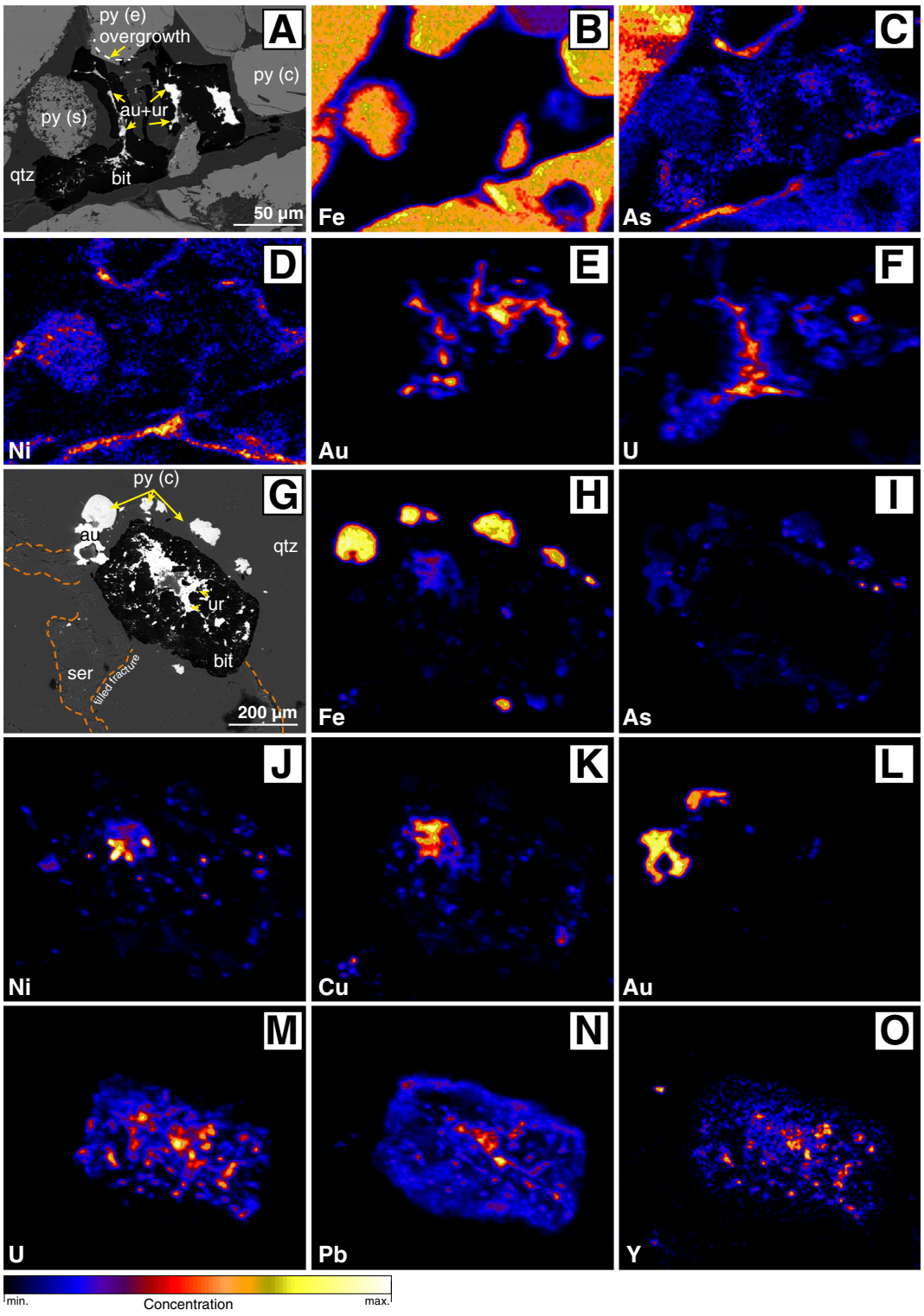

Fig. 10. (A) Back-scattered electron image showing native gold and uranium in pyrobitumen. (B–F) Micro-PIXE maps showing the distribution of Fe, As, Ni, Au and U of the area shown in A. (G) Back-scattered electron image showing uranium in a pyrobitumen nodule and adjacent native gold and pyrite grains in surrounding authigenic quartz. (H–O) Micro-PIXE maps showing the distribution of Fe, As, Ni, Cu, Au, U, Pb and Y in the area shown in G. Some of the gold occurs in pyrite, whereas U, Pb, Y occur within the pyrobitumen nodule. Fractures in the quartz matrix are highlighted by dashed, orange lines. Abbreviations: au = native gold; qtz = quartz; py (c) = compact pyrite; py (e) = epigenetic pyrite; py (s) = sooty pyrite; ser = sericite; ur = uraninite. (For interpretation of the references to colour in this figure legend, the reader is referred to the web version of this article.).

uranium in the concretionary pyrite would be consistent with the broad nature of the U peaks observed in the LA–ICP–MS line scan (Fig. 7B). The delicate internal structure of this pyrite and its abundance in the East and West Rand sub-basins indicate that it experienced limited sedimentary transport and therefore formed relatively close to its site of deposition.

6.3. Evidence for hydrothermal fluids

Cathodoluminescence imaging of quartz and associated minerals in the Black Reef makes it possible to discern a history starting with the deposition of detrital quartz and culminating with the infiltration of fluids during metamorphism. The cathodoluminescence images help distinguish several different types of detrital quartz grains that were likely derived from different igneous sources, and authigenic quartz, which is interpreted to have cemented them during diagenesis (Fig. 4A and B). They also show that the authigenic quartz was cut by numerous fractures created during metamorphism and subsequently healed (Fig. 4 E, F, G and H), implying possible fluid infiltration. Such infiltration is further indicated by large fibrous strain fringes of quartz developed in the pressure shadows of rigid grains and in veins (Fig. 4K). This infiltration created dilation sites (secondary porosity) that supported the movement of fluids in the sediment, and led to the formation of secondary minerals such as sericite and fine-grained quartz (as chert or opal) along veins and fractures zones (Fig. 4J, K). The presence of small veinlets and nodules of pyrobitumen in them (Fig. 4E, F, G, H and J) indicate, moreover, that the aqueous fluids were accompanied by liquid hydrocarbons. Luminescent radiation damage in the zones of hydrothermal activity (Fig. 4E–H) provides evidence for a concomitant introduction of uranium and possibly gold.

6.4. Gold and uranium transport and deposition

Textural evidence for a non-detrital origin of the gold is provided by the occurrence of native gold in (i) fractures and pore spaces of pyrite, (ii) as rims around pyrite and (iii) and around pyrobitumen (Fig. 3A–F; 10A, E, L; Fig. A.1). In all these modes of occurrence, the gold is texturally late in the paragenetic sequence and associated with a sericite- and pyrobitumen-bearing vein/fracture system within the authigenic quartz matrix. Evidence that the uranium mineralisation is also not detrital is its development as finely dispersed irregularly shaped uraninite grains and secondary U-bearing minerals in pyrobitumen nodules and veinlets that commonly contain native gold (Fig. 3E, F; 10A, G). Finally, both metals are present in elevated concentrations in epigenetic pyrite overgrowths on detrital pyrite (Fig. 7B).

The presence of native gold in pyrite and pyrobitumen suggests that its precipitation from the hydrothermal ore fluid(s) was controlled by these phases. In the case of pyrite, this is further suggested by micro-PIXE elemental maps, line-scans and spot analyses, which show that the gold was deposited adjacent to zones that are arsenic-rich and have neighbouring nickel-rich zones (Fig. 9). According to experiments by Möller and Kersten (1994), pyrite of this composition can act as a self-driving galvanic cell in which the As-rich zones represent p-type semiconductors (cathode) and the Co–Ni-rich zones n-type semiconductors (anode). More importantly, electric potentials developed in these mixed-type semi-conductors are sufficient to induce electrochemical precipitation, even from dilute solutions. The presence of sericite in the veins indicates weakly acidic conditions in which $AuHS^0$ and $Au(HS)_2^-$ would have been stable. Within the galvanic cell, the gold bisulphide species would dissociate to Au^+ and HS^-, and the cathode would act as an electron donor, reducing the Au^+ to metallic gold (Au^0).

It is also possible that the association of gold and at least the secondary pyrite could reflect destabilisation of the gold bisulphide complexes due to sulphidation (Williams-Jones et al., 2009; Williams-Jones and Migdisov, 2014). Indeed, this possibility is suggested by the sulphur and iron isotopic study of Hofmann et al. (2009) of pyrite separates from the Black Reef, which showed that some of the pyrite could be derived from the sulphidation of pre-existing iron oxide (or iron silicate) minerals, such as magnetite or ilmenite.

The strong correlation between dendritic and partially intergrown gold and uranium minerals (Fig. 10A, E, F) shows that both metals were introduced into the Black Reef together. In contrast to the older conglomeratic reefs of the Witwatersrand Supergroup, detrital uraninite is absent from the ~ 2.59 Ga Black Reef. This implies that by the time of formation of the Black Reef, the oxygen level of the atmosphere was sufficient to oxidize insoluble uraninite. Under these conditions, uranium could have been transported in aqueous solutions as uranyl-complexes. In the case of both the gold and uranium, the association of the metals with pyrobitumen could indicate that they were deposited as native gold and uraninite, respectively, as a result of reduction of the hydrothermal fluid by the organic matter. However, as shown by Fuchs et al. (2015), pyrobitumen in the Carbon Leader reef of the Witwatersrand Supergroup contains nanoparticles of uraninite, and is interpreted by them to reflect transport of uranium by liquid hydrocarbons. It is therefore equally possible that the pervasive and diffuse distribution of uranium- and radiogenic lead in the pyrobitumen of the Black Reef (Fig. 10 M, N) and radiation damage of adjacent quartz (strong luminescence; Fig. 4D, E and G) may be better explained by the transport of uranium in liquid hydrocarbons.

Epigenetic pyrite overgrowths around detrital cores produced by post-depositional hydrothermal fluids also contributed gold and uranium to the total resource of the Black Reef. Owing to the small size of the overgrowths, it was not possible to conduct reliable analyses of the concentration of gold and uranium in them. However, time-resolved LA–ICP–MS line scans along pyrite grains (Fig. 7B) with detrital cores and epigenetic overgrowths, indicate approximate gold and uranium concentrations in the overgrowths of 1362 ppm and 698 ppm, respectively.

Two recent studies of the Witwatersrand Au–U deposits have proposed the syngenetic concentration of gold by volcanic rain, rivers, groundwater, shallow seas and microbial life (Frimmel and Hennigh, 2015; Heinrich, 2015). These studies envisage that the gold entered the basin in dissolved form and precipitated due to interaction with microbial mats. Whether or not these studies satisfactorily explain the concentration of gold in the Witwatersrand reefs, the results of the present study suggest strongly that gold and uranium concentration in the Black Reef Formation was effected by post-depositional aqueous and organic fluids. The Black Reef lacks evidence of the former existence of microbial mats, and the organic matter that is present is texturally late, occurring as pyrobitumen veins and nodules, which are best explained as being the residues of liquid hydrocarbons. Moreover, both the gold and uraninite occur exclusively in healed fractures, as rims on pyrite, and in epigenetic pyrite overgrowths.

6.5. A model for the Au–U mineralisation of the Black Reef

Based on the data that have been presented in this paper, we propose a genetic model in which the detrital components of the Black Reef Formation were derived from the hinterland immediately surrounding the basin and not from erosion of underlying Witwatersrand strata. In the case of the detrital pyrite, provenance analyses clearly rule out these strata as the source of either the compact or concretionary/sooty varieties. We propose, instead, that the compact variety was derived from felsic and mafic volcanic rocks in greenstone belts, possibly associated with orogenic gold deposits, and that the concretionary/sooty varieties came from organic-rich shales in the Black Reef Basin from which they incorporated trace elements, including gold and uranium. The irregular to dendritic nature of the economic gold and uranium mineralisation shows clearly that it is not detrital in origin (because of the age of the deposit, 2.59 Ga, which coincides roughly with the onset of the great oxidation event, uraninite is unlikely to have been stable in the surficial environment; Henry and Master, 2008, Holland, 2006). On the contrary, its close association with pyrite and pyrobitumen (the gold occurs commonly in fractures within the two phases and uranium is largely restricted to the pyrobitumen) suggests strongly that the metals were deposited from hydrothermal fluids or, in the case of uranium, possibly from liquid hydrocarbons. Significantly, however, the Black Reef only contains economic concentrations of gold and uranium where it is underlain by auriferous and uraniferous

Witwatersrand strata. We therefore propose that gold and uranium were recycled from these reefs into the Black reef, not mechanically as has been proposed previously, but by hydrothermal fluids or, in the case of uranium, possibly by hydrocarbon liquids. According to this model, low-grade regional metamorphism promoted the circulation of hydrothermal and hydrocarbon fluids between the two sedimentary successions, with the upward migration of the fluids creating the porosity needed to introduce gold and uranium into the lithified conglomerates of the Black Reef. The gold is interpreted to have been transported as a bisulphide complex(es) in the hydrothermal fluid and deposited electrochemically on pyrite, in pyrobitumen due to the resulting destabilisation of the bisulphide (reduction), or, in part, possibly as a consequence of sulphidation of iron oxide/iron-bearing silicate minerals (neo-formed pyrite). The uraninite was deposited either from hydrothermal fluids as a result of the reduction of U^{6+} to U^{4+} by hydrocarbons or directly from hydrocarbon liquids via nanocrystalline growth and flocculation. Both metals were also concentrated as trace elements in the hydrothermally formed epigenetic pyrite overgrowth.

Supplementary data to this article can be found online at http://dx.doi.org/10.1016/j.oregeorev.2015.07.010.

Conflict of interest

The authors declare that there is no conflict of interest according to the publishing ethics policy of the journal.

Acknowledgements

The authors thank the staff of the core library of the Council of Geoscience (South Africa), AngloGold Ashanti, Pamodzi Gold, GoldOne Ltd. and Harmony Gold for the supply of samples. Simon Jackson and colleagues of the Geological Survey of Canada provided invaluable help with the LA–ICP–MS analyses and their interpretation, and the staff of iThemba labs with the PIXE analyses. Financial support for the research was provided by a NSERC Discovery grant to AEW-J.

References

Agangi, A., Hofmann, A., Wohlgemuth-Ueberwasser, C.C., 2013. Pyrite zoning as a record of mineralization in the ventersdorp contact reef, Witwatersrand Basin, South Africa. Econ. Geol. 108, 1243–1272.

Armstrong, R.A., Compston, W., Retief, E.A., Williams, I.S., Welke, H.J., 1991. Zircon ion microprobe studies bearing on the age and evolution of the Witwatersrand triad. Precambrian Res. 53, 243–266.

Barnicoat, A.C., Henderson, I.H.C., Knipe, R.J., Yardley, B.W.D., Napier, R.W., Fox, N.P.C., Kenyon, A.K., Muntingh, D.J., Strydom, D., Winkler, K.S., Lawrence, S.R., Cornford, C., 1997. Hydrothermal gold mineralization in the Witwatersrand basin. Nature 386, 820–824.

Barton, E.S., Hallbauer, D.K., 1996. Trace-element and U–Pb isotope compositions of pyrite types in the Proterozoic Black Reef, Transvaal Sequence, South Africa: Implications on genesis and age. Chem. Geol. 133, 173–199.

Button, A., 1973. A regional study of the stratigraphy and development of the Transvaal basin in the eastern and northeastern Transvaal (Ph.D. Thesis) University of the Witwatersrand, Johannesburg.

Churms, C., Pilcher, J., Springhorn, K., Tapper, U., 1993. A VAX and PC-based data acquisition system for MCA, scanning and list-mode analysis. Nucl. Instrum. Meth. B 77, 56–71.

Churms, C., Prozesky, V., Springhorn, K., 1999. The remote control of nuclear microprobes over the Internet. Nucl. Instrum. Meth. B 158, 124–128.

Clendenin, C.W., Henry, G., Charlesworth, E.G., 1991. Characteristics of and influences on the Black Reef depositional sequence in the eastern Transvaal. S. Afr. J. Geol. 94, 321–327.

Coveney, R.M., 2000. Metalliferous shales and the role of organic matter, with examples from China, Poland, and the United States. Rev. Econ. Geol. 9, 251–280.

Coward, M.P., Spencer, R.M., Spencer, C.E., 1995. Development of the Witwatersrand Basin, South Africa. Geol. Soc. Lond. Spec. Publ. 95, 243–269.

Drennan, G.R., Robb, L.J., 2006. The nature of hydrocarbons and related fluids in the Witwatersrand Basin, South Africa: their role in metal redistribution. Geol. Soc. Am. Spec. 405, 353–385.

Els, B.G., Vandenberg, W.A., Mayer, J.J., 1995. The Black Reef Quartzite formation in the Western Transvaal — sedimentological and economic-aspects, and significance for basin evolution. Miner. Deposita 30, 112–123.

Eriksson, P.G., Reczko, B.F.F., 1995. The sedimentary and tectonic setting of the Transvaal Supergroup floor rocks to the Bushveld complex. J. Afr. Earth Sci. 21, 487–504.

Eriksson, P.G., Altermann, W., Hartzer, F.J., 2006. The Transvaal supergroup and precursors. In: Johnson, M.R., Anhaeusser, C.R., Thomas, R.J. (Eds.), The Geology of South Africa. Geol. Society of South Africa, Johannesburg, pp. 237–260.

Frankel, J.J., 1940. Notes on some of the minerals in the Black Reef series. Trans. Geol. Soc. S. Afr. 43, 1–11.

Frey, M., 1988. Zur Metallogenese von Gold-Uran Paläoseifen in der Black Reef Formation der Transvaal-Supergruppe Südafrika (PhD Thesis) University of Cologne, Cologne.

Frey, M., Germs, G.J.B., Oberthuer, T., Saager, R., 1991. Textural and compositional characteristics of gold, sulphides and tourmaline in the black reef Palaeoplace, Transvaal sequence, South Africa. Internal Research Report. University of Cologne.

Frimmel, H.E., 1994. Metamorphism of Witwatersrand Gold. Explor. Min. Geol. 3, 357–370.

Frimmel, H.E., 1997. Detrital origin of hydrothermal Witwatersrand gold — a review. Terra Nova 9, 192–197.

Frimmel, H., Hennigh, Q., 2015. First whiffs of atmospheric oxygen triggered onset of crustal gold cycle. Miner. Deposita 50, 5–23.

Frimmel, H.E., Groves, D.I., Kirk, J., Ruiz, J., Chezley, J., Minter, W.E.L., 2005. The formation and preservation of the Witwatersrand Goldfields, the world's largest gold province. In: Hedenquist, J.W., Thompson, J.F.H., Goldfarb, R.J., Richards, J.P. (Eds.), One Hundreth Anniversary Volume. Society of Economic Geologists, Inc., Littleton, Colerado, pp. 769–797.

Frimmel, H.E., Zeh, A., Lehrmann, B., Hallbauer, D., Frank, W., 2009. Geochemical and geochronological constraints on the nature of the immediate basement next to the Mesoarchaean Auriferous Witwatersrand Basin, South Africa. J. Petrol. 50, 2187–2220.

Fuchs, S., Schumann, D., Williams-Jones, A.E., Vali, H., 2015. The growth and concentration of uranium and titanium minerals in hydrocarbons of the Carbon Leader Reef, Witwatersrand Supergroup, South Africa. Chem. Geol. 393–394, 55–66.

Germs, G.J.B., 1982. A paleogeographical study of the Black Reef Formation of the Transvaal Supergroup in the Venterdorp–Balfour area. J.C.I. — Company Report No. 136.

Graton, L.C., 1930. Hydrothermal origin of the Rand Gold Deposits; Part 1, testimony of the conglomerates. Econ. Geol. 25, 1–185.

Heinrich, C.A., 2015. Witwatersrand gold deposits formed by volcanic rain, anoxic rivers and Archaean life. Nat. Geosci. 8, 206–209.

Henry, G., Master, S., 2008. Black Reef Project. Council for Scientific and Industrial Research (CSIR) and University of the Witwatersrand, Johannesburg.

Henry, G., Clendenin, C.W., Charlesworth, E.G., 1990. Depositional facies of the Black Reef Quartzite Formation in the eastern Transvaal. 23rd Earth Science Congress ed.. Geological Society of South Africa, Cape Town, pp. 230–233.

Hofmann, A., Bekker, A., Rouxel, O., Rumble, D., Master, S., 2009. Multiple sulphur and iron isotope composition of detrital pyrite in Archaean sedimentary rocks: A new tool for provenance analysis. Earth Planet. Sc. Lett. 286, 436–445.

Holland, H.D., 2006. The oxygenation of the atmosphere and oceans. Philos. T. Roy. Soc. B. 361, 903–915.

Jochum, K.P., Wilson, S.A., Abouchami, W., Amini, M., Chmeleff, J., Eisenhauer, A., Hegner, E., Iaccheri, L.M., Kieffer, B., Krause, J., Mcdonough, W.F., Mertz-Kraus, R., Raczek, I., Rudnick, R.L., Scholz, D., Steinhoefel, G., Stoll, B., Stracke, A., Tonarini, S., Weis, D., Weis, U., Woodhead, J.D., 2011. GSD-1G and MPI-DING Reference Glasses for In Situ and Bulk Isotopic Determination. Geostand. Geoanal. Res. 35, 193–226.

Kirk, J., Ruiz, J., Chesley, J., Walshe, J., England, G., 2002. A major archean, gold- and crust-forming event in the Kaapvaal craton, South Africa. Science 297, 1856–1858.

Koglin, N., Frimmel, H.E., Minter, W.E.L., Bratz, H., 2010. Trace-element characteristics of different pyrite types in Mesoarchaean to Palaeoproterozoic placer deposits. Miner. Deposita 45, 259–280.

Large, R.R., Maslennikov, V.V., Robert, F., Danyushevsky, L.V., Chang, Z., 2007. Multistage Sedimentary and Metamorphic Origin of Pyrite and Gold in the Giant Sukhoi Log Deposit, Lena Gold Province, Russia. Econ. Geol. 102, 1233–1267.

Large, R.R., Bull, S.W., Maslennikov, V.V., 2011. A carbonaceous sedimentary source-rock model for carlin-type and orogenic gold deposits. Econ. Geol. 106, 331–358.

Large, R.R., Meffre, S., Burnett, R., Guy, B., Bull, S., Gilbert, S., Goemann, K., Danyushevsky, L., 2013. Evidence for an intrabasinal source and multiple concentration processes in the formation of the Carbon Leader Reef, Witwatersrand Supergroup, South Africa. Econ. Geol. 108, 1215–1241.

Law, J.D.M., Phillips, G.M., 2005. Hydrothermal replacement model for Witwatersrand Gold. In: Hedenquist, J.W., Thompson, J.F.H., Goldfarb, R.J., Richards, J.P. (Eds.), One Hundreth Anniversary Volume. Society of Economic Geologists, Inc., Littleton, Colorado, pp. 799–811.

Martin, D.M., Clendenin, C.W., Krapez, B., Mcnaughton, N.J., 1998. Tectonic and geochronological constraints on late Archaean and Palaeoproterozoic stratigraphic correlation within and between the Kaapvaal and Pilbara Cratons. J. Geol. Soc. Lond. 155, 311–322.

Meyer, F.M., Robb, L.J., 1996. The geochemistry of black shales from the Chuniespoort group, Transvaal sequence, eastern Transvaal, South Africa. Econ. Geol. Bull. Soc. 91, 111–121.

Minter, W.E.L., 2006. The sedimentary setting of Witwatersrand placer mineral deposits in an Archean atmosphere. Geol. Soc. Am. Mem. 198, 105–119.

Minter, W.E.L., Goedhart, M., Knight, J., Frimmel, H.E., 1993. Morphology of Witwatersrand Gold Grains from the Basal Reef — Evidence for Their Detrital Origin. Econ. Geol. Bull. Soc. 88, 237–248.

Möller, P., Kersten, G., 1994. Electrochemical accumulation of visible gold on pyrite and arsenopyrite surfaces. Miner. Deposita 29, 404–413.

Obbes, A.M., 2000. The structure, stratigraphy and sedimentology of the Black Reef-Malmani-Rooihoogte succession of the Transvaal Supergroup southwest of Pretoria. Bull. Counc. Geosci. 127, 89.

Papenfus, J.A., 1964. The Black Reef Series within the Witwatersrand basin with special reference to its occurrence at Government Gold mining areas. In: Haughton, S.H.

(Ed.), Some are deposits in South Africa. Geological Society of South Africa, pp. 191–218.
Phillips, G.N., 1988. Widespread Fluid Infiltration during Metamorphism of the Witwatersrand Goldfields — Generation of Chloritoid and Pyrophyllite. J. Metamorph. Geol. 6, 311–332.
Phillips, G.N., Law, J.D.M., 1994. Metamorphism of the Witwatersrand Gold Fields — a review. Ore Geol. Rev. 9, 1–31.
Phillips, G.N., Myers, R.E., 1989. The Witwatersrand Gold Fields: part II. An Origin for Witwatersrand Gold during metamorphism and associated alteration. In: Keays, R.R., Ramsay, W.R.H., Groves, D.I. (Eds.), The Geology of gold deposits: the perspective in 1988. Society of Economic Geologists, New Haven, pp. 598–608.
Phillips, G.N., Law, J.D.M., Stevens, G., 1997. Alteration, heat, and Witwatersrand gold: 111 years after Harrison and Langlaagte. S. Afr. J. Geol. 100, 377–392.
Piper, D.Z., Calvert, S.E., 2009. A marine biogeochemical perspective on black shale deposition. Earth Sci. Rev. 95, 63–96.
Pretorius, D.A., 1991. The souces of Witwatersrand gold and uranium: a continued difference of opinion. Econ. Geol. Monogr, New Haven.
Prozesky, V.M., Przybylowicz, W.J., Vanachterbergh, E., Churms, C.L., Pineda, C.A., Springhorn, K.A., Pilcher, J.V., Ryan, C.G., Kritzinger, J., Schmitt, H., Swart, T., 1995. The Nac nuclear microprobe facility. Nucl. Instrum. Meth. B 104, 36–42.
Ramdohr, P., 1958. Die Uran- und Goldlagerstätten Witwatersrand-Blind River District-Dominion Reef - Serra de Jacobina: Erzmikroskopische Untersuchungen und ein geologischer Vergleich. Akedamie Verlag, Berlin.
Reich, M., Kesler, S.E., Utsunomiya, S., Palenik, C.S., Chryssoulis, S.L., Ewing, R.C., 2005. Solubility of gold in arsenian pyrite. Geochim. Cosmochim. Acta 69, 2781–2796.
Robb, L.J., Meyer, F.M., 1995. The Witwatersrand Basin, South Africa: geological framework and mineralization processes. Ore Geol. Rev. 10, 67–94.
Ryan, C.G., 2000. Quantitative trace element imaging using PIXE and the nuclear microprobe. Int. J. Imaging Syst. Technol. 11, 219–230.
Ryan, C.G., Jamieson, D.N., 1993. Dynamic analysis — online quantitative pixe microanalysis and its use in overlap-resolved elemental mapping. Nucl. Instrum. Meth. B 77, 203–214.
Ryan, C.G., Cousens, D.R., Sie, S.H., Griffin, W.L., Suter, G.F., Clayton, E., 1990. Quantitative pixe microanalysis of geological material using the csiro proton microprobe. Nucl. Instrum. Meth. B 47, 55–71.
Ryan, C.G., Jamieson, D.N., Churms, C.L., Pilcher, J.V., 1995. A new method for online true-elemental imaging using pixe and the proton microprobe. Nucl. Instrum. Meth. B 104, 157–165.
Saager, R., 1970. Structures in pyrite from the Basal Reef in the Orange Free State Goldfield. Trans. Geol. Soc. S. Afr. 73, 30–46.
Spellman, R.L., 1986. Northeast prospect (NEP) shaft high grade gold placer: a feeder channel into the East Rand Black Reef, Geocongress '86. Geol. Soc. S. Afr. 985–988.
Swiegers, J.U., 1939. Gold, carbon, pyrite and other sulphides in the Black Reef. Trans. Geol. Soc. S. Afr. 42, 35–46.
Utter, T., 1978. Morphology and geochemistry of different pyrite types from the Upper Witwatersrand System of the Klerksdorp Goldfield, South Africa. Geol. Rundsch. 67, 774–804.
Williams-Jones, A.E., Migdisov, A.A., 2014. Experimental constraints on the transport and deposition of metals in ore-forming hydrothermal systems. In: Kelley, K.D., Howard, C.G. (Eds.), Building Exploration Capability for the 21st Century, 18 ed.. Society of Economic Geologists, pp. 77–95.
Williams-Jones, A.E., Bowell, R.J., Migdisov, A.A., 2009. Gold in solution. Elements 5, 281–287.
Wilson, S.A., Ridley, W.I., Koenig, A.E., 2002. Development of sulfide calibration standards for the laser ablation inductively-coupled plasma mass spectrometry technique. J. Anal. At. Spectrom. 17, 406–409.
Wood, S.A., 1996. The role of humic substances in the transport and fixation of metals of economic interest (Au, Pt, Pd, U, V). Ore Geol. Rev. 11, 1–31.
Wronkiewicz, D.J., Condie, K.C., 1987. Geochemistry of Archean shales from the Witwatersrand Supergroup, South Africa — Source-area weathering and provenance. Geochim. Cosmochim. Acta 51, 2401–2416.